MASARYKOVA UNIVERZITA
Přírodovědecká fakulta
Ústav teoretické fyziky a astrofyziky

Diplomová práce

Brno 2026 **Samuel Fabo**

MASARYKOVA
UNIVERZITA
PŘÍRODOVĚDECKÁ FAKULTA
ÚSTAV TEORETICKÉ FYZIKY A ASTROFYZIKY

Studium vybraných excentrických zákrytových dvojhězd

Diplomová práce

Samuel Fabo

Vedoucí práce: doc. RNDr. Miloslav Zejda, Ph.D.
Brno 2026

Bibliografický záznam

Autor:	Samuel Fabo Přírodovědecká fakulta, Masarykova univerzita Ústav teoretické fyziky a astrofyziky
Název práce:	Studium vybraných excentrických zákrytových dvojhězd
Studijní program:	Fyzika
Studijní obor:	Astrofyzika
Vedoucí práce:	doc. RNDr. Miloslav Zejda, Ph.D.
Akademický rok:	2025/26
Počet stran:	VIII + 50
Klíčová slova:	Zákrytové dvojhvězdy; Fotometrie; Světelná křivka; $O-C$ diagram; TESS; ASAS-SN; Apsidální pohyb

Bibliographic Entry

Author:	Samuel Fabo Faculty of Science, Masaryk University Department of Theoretical Physics and Astrophysics

Title of Thesis:	Study of selected eccentric eclipsing binaries
Degree Programme:	Physics
Field of Study:	Astrophysics
Supervisor:	doc. RNDr. Miloslav Zejda, Ph.D.
Academic Year:	2025/26
Number of Pages:	VIII + 50
Keywords:	Eclipsing binaries; Photometry; Light curve; $O-C$ diagram; TESS; ASAS-SN; Apsidal motion

Abstrakt

Excentrické zákrytové dvojhvězdy slouží jako klíčové astrofyzikální laboratoře, které prostřednictvím pozorování apsidálního pohybu umožňují přímé testování teoretických modelů vnitřní stavby a vývoje hvězd. Tato práce zkoumala pět excentrických zákrytových dvojhvězd: V919 Cep, AT Lep, CF Mon, 2MASS J10024347-5643283 a 2MASS J08453462-2158013. Byla analyzována dostupná fotometrická data z přehlídek. Hlavním a referenčním zdrojem dat byla družice TESS, doplněná o přehlídku ASAS-SN a další. Ze zkonstruovaných světelných křivek byly určeny okamžiky minim a z nich byly následně sestaveny $O-C$ diagramy. Efemeridy objektů byly na základě $O-C$ diagramů opraveny. Fyzikální modely byly analyzovány a parametry objektů byly určeny pomocí programu PHOEBE. V systému V919 Cep byl detekován apsidální pohyb s periodou 74.1 let. Fitováním $O-C$ diagramu bylo možné určit parametry potřebné k výpočtu konstanty vnitřní struktury. Spolu s teoretickou hodnotou byly konstanty porovnány s jinými objekty a bylo zjištěno, že do daného vzorku zapadají.

Abstract

Eccentric eclipsing binary stars serve as key astrophysical laboratories that, through the observation of apsidal motion, allow for the direct testing of theoretical models of internal stellar structure and evolution. This thesis examined five eccentric eclipsing binaries: V919 Cep, AT Lep, CF Mon, 2MASS J10024347-5643283, and 2MASS J08453462-2158013. Available photometric data from surveys were analyzed. The main and reference source of data was the TESS satellite, supplemented by the ASAS-SN survey and others. From the constructed light curves, the minima timings were determined, and $O-C$ diagrams were constructed from them. The ephemerides for the objects were corrected based on the $O-C$ diagrams. Physical models were analyzed, and object parameters were determined using the PHOEBE program. Apsidal motion with a period of 74.1 years was detected in the V919 Cep system. By fitting the $O-C$ diagram, we were able to determine the parameters needed to calculate the internal structure constants. The constants were compared with those of other objects, along with their theoretical values, and were found to fit the sample.

MASARYKOVA UNIVERZITA
PŘÍRODOVĚDECKÁ FAKULTA
KOTLÁŘSKÁ 2, 611 37 BRNO
IČ: 00216224
DIČ: CZ00216224

ZADÁNÍ DIPLOMOVÉ PRÁCE

Akademický rok: 2025/2026

Ústav:	Ústav teoretické fyziky a astrofyziky
Student:	Bc. Samuel Fabo
Program:	Fyzika
Specializace:	Astrofyzika

Ředitel *ústavu* PřF MU Vám ve smyslu Studijního a zkušebního řádu MU určuje diplomovou práci s názvem:

Název práce:	Studium vybraných excentrických dvojhvězd
Název práce anglicky:	Study of eccentric eclipsing binaries
Jazyk práce:	angličtina

Oficiální zadání:
Hvězdy, zejména určitých typů, preferují dvojhvězdné uspořádání. Složky dvojhvězdy obíhají kolem společného těžiště většinou pro kruhových trajektoriích. Vyskytují se ale i dvojhvězdy s excentrickými trajektoriemi. Cílem diplomové práce je detailní studium vybraných excentrických zákrytových dvojhvězd. Na základě dostupných dat a vlastních pozorování
Student provede detailní analýzu a pomocí modelu s využitím dostupných programů jako PHOEBE určí základní fyzikální parametry složek soustav. Pokusí se také stanovit koeficient vnitřní struktury složek. Výsledky porovná s obdobnými již studovanými dvojhvězdami.

Vedoucí práce:	doc. RNDr. Miloslav Zejda, Ph.D.
Konzultant:	Mgr. Jakub Kolář, Ph.D.
Datum zadání práce:	28. 11. 2024
V Brně dne:	28. 4. 2026

Zadání bylo schváleno prostřednictvím IS MU.

Bc. Samuel Fabo, 28. 11. 2024
doc. RNDr. Miloslav Zejda, Ph.D., 28. 11. 2024
Mgr. Dušan Hemzal, Ph.D., 29. 11. 2024

Poděkování

Na tomto místě bych chtěl poděkovat svému vedoucímu práce doc. RNDr. Miloslavu Zejdovi, Ph.D. a konzultantovi Mgr. Jakubovi Kolářovi Ph.D. za cenné rady, vstřícný přístup a čas, který mi věnovali při konzultacích a počas celého psaní této práce. Rád bych také poděkoval celé rodině a své přítelkyni za podporu během celého studia.

Prohlášení

Prohlašuji, že jsem svoji diplomovou práci vypracoval samostatně pod vedením vedoucího práce a konzultanta s využitím informačních zdrojů, které jsou v práci citovány.

Brno 4. května 2026 .....

Samuel Fabo

Contents

Chapter 1

Insight into the topic

1.1 Motivation

A fundamental objective of modern stellar astrophysics is to understand the formation, internal structure, evolutionary pathways of stars, and even the demise of stars. Binary and multiple systems serve as natural laboratories for testing stellar theory because their mutual gravitational interactions enable direct measurements of fundamental stellar parameters. These parameters are essential for calibrating stellar evolutionary models and for studying populations that give rise to compact objects and gravitational-wave sources.

Eclipsing binaries (EBs) are especially valuable. Their periodic eclipses provide precise constraints on orbital inclination, stellar proportion, and orbital eccentricity. Combined with radial velocity data, they provide absolute masses and radii with unmatched accuracy (Torres et al., 2010). An even richer diagnostic potential is offered by eccentric eclipsing binaries (EEBs) systems with non-circular orbits. With the advent of modern photometric surveys and high-resolution spectroscopy, the number of well-characterized EEBs has grown substantially. Orbital precession, so-called apsidal motion, is caused by tidal and rotational distortions, as well as general relativistic effects. This motion directly probes the internal mass distribution of the stars. The Newtonian component of this motion depends on the internal structure constant (k_2), a measure of central mass concentration. This fact makes EEBs useful for testing stellar structure models (Claret and Gimenez, 2010).

This thesis contains a detailed analysis of selected eccentric eclipsing binary systems. Models based on software such as PHOEBE are used to determine the fundamental physical parameters of the stellar components, such as their masses, radii, and effective temperatures. The internal structure constant of each component is also estimated to provide insight into its mass distribution. The results obtained in this thesis are compared with those of previously studied binary systems in order to evaluate consistency and identify potential evolutionary differences.

1.2 Binary stars

At first sight of the night sky, the universe appears to be made up of a hundred or thousands of lonely stars. However, our Galaxy alone contains over 100 billion stars; some sources estimate as many as 400 billion. Furthermore, many stars prioritize 'living' with a companion, forming binary stars (binaries). The components of a binary star are gravitationally bound objects orbiting a common center of mass located at the focus of the elliptical orbits (see Figure 1.1). It is thus a classic Keplerian two-body problem with a central force.

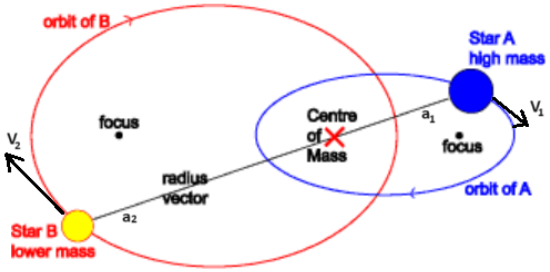

Figure 1.1: Schema of the binary star configuration.(Australian Telescope National Facility)

Binaries allow us to explore the universe more easily than lonely stars because it is easier to determine the basic parameters of the components themselves, such as mass M, radius R, period of rotation T, luminosity L, or even the system's parameters, such as the mutual distance a and the orbital period P. With the above statement, we can easily combine fundamental quantities into Kepler's third law:

$$\frac{a^3}{P^2} = \frac{G(M_1 + M_2)}{4\pi^2}, \tag{1.1}$$

where G is the gravitational constant.

In general, the periods of these systems may be different. There are recorded cases of periods lasting a few minutes, but we also know of objects with periods of up to several decades.

There are three angles that are important when studying the orbits of binary stars. If we know the argument of the periastron (ω), the inclination (i), and the longitude of the ascending node (Ω), we can characterize the orientation of the system in three-dimensional space (Figure 1.2). The angle ω is the angle between the ascending node and the direction of the periastron. It is measured in the orbital plane in the direction of orbital motion. In binary star systems, the i is the angle between the normal of the orbital plane and the observer's plane. The inclination value determines whether we can observe binary eclipses from Earth. The parameter (Ω) is the angle between the true north and the ascending node, where the ascending node (N+) is defined as the node at which the primary star is observed to move away from the observer while passing through the plane of the sky (Sana and Vrancken, 2025). If we add these three angles to the major semi-major axis, period, and eccentricity, we get a full description of the system's orbit.

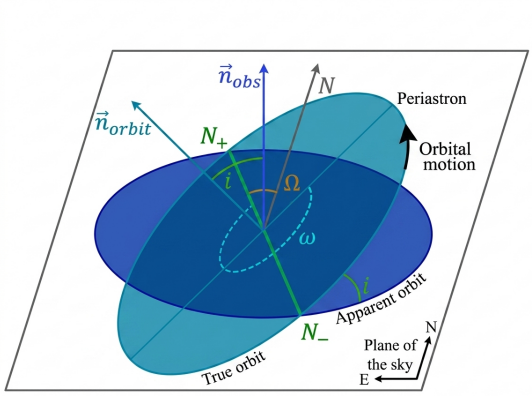

Figure 1.2: Geometry of an orbit. Taken and modified from Sana and Vrancken (2025).

1.3 Eclipsing binary stars

The orbital plane of a binary star can be oriented at any angle relative to the line of sight, as this depends primarily on the initial conditions at the formation of the entire system. A specific case involves systems where stars overlap each other during their orbit relative to the observer. We call this type of system an eclipsing binary, and they are a very valuable source of information. For an eclipse to occur, the following condition must be fulfilled:

$$\sin\phi \leq \frac{R_1 + R_2}{a}, \tag{1.2}$$

where R_1 and R_2 are the radii of the stars, and a is the semi-major axis. The ϕ is the angle between the observer and the plane of orbit and is defined by the system's inclination (Figure 1.2): $\phi = 90° - i$.

The condition 1.2 defines only a partial eclipse. A total eclipse occurs mainly when the inclination is close to 90° or when there is a large difference in the sizes of the components:

$$\sin\phi \leq \frac{|R_1 - R_2|}{a}. \tag{1.3}$$

Once one of the conditions (1.2, 1.3) is satisfied, we observe a periodic change in luminous flux over time and plot it as a light curve. Binary stars typically exhibit two decreases in brightness per complete orbit, or in other words, per period. A *primary* eclipse is deeper and usually occurs when a hotter star moves into the background, and a cooler star is in the foreground. A *secondary* eclipse is therefore the opposite and occurs when the cooler star moves behind the hotter one, as can be seen in Figure 1.3 (Tauris and van den Heuvel, 2023).

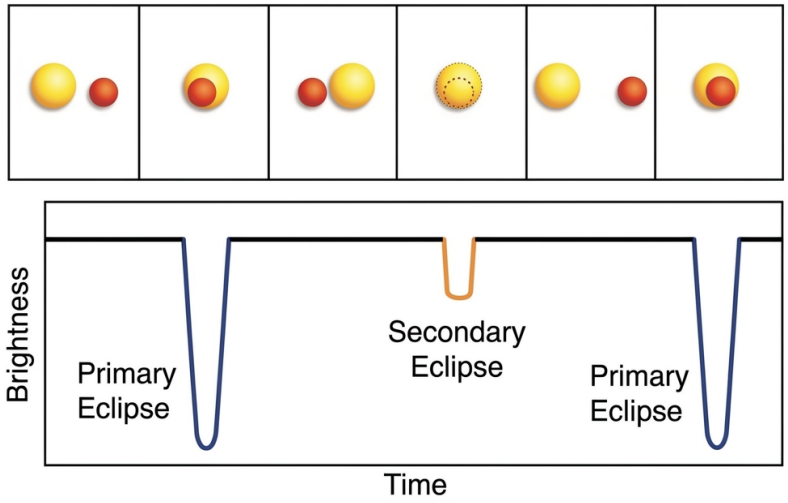

Figure 1.3: Schematic light curve and explanation of eclipses. The yellow star is considered hotter. Taken and edited from: www.cosmosatyourdoorstep.com.

This figure illustrates eclipses, but the appearance of the light curve varies from system to system. The shape of the curve is a direct result of the properties of the stars and the system. For this reason, binary stars began to be classified based on the morphology of their light curves.

The names of the individual categories were historically derived from the first observed systems of a certain type. The first eclipsing binary star ever discovered was β *Persei*, which was named Algol. An *Algol*-type binaries are characterized by almost constant brightness between eclipses. The tidal forces between components are not strong, and therefore the stars are spherical or slightly ellipsoidal. The eclipses are clearly defined, and there is usually a depth difference between the primary and secondary stars (Tauris and van den Heuvel, 2023).

The other two categories are quite similar in terms of their light (Figure 1.4). Both have rounded minima and maxima in brightness. This makes it impossible to determine the start and end of the eclipse. However, there are differences, for example, in the depth of the eclipses themselves. The β *Lyrae* type has significantly different minimum depths. The system consists of components strongly influenced by tidal forces, which are deformed into ellipsoids. As the stars move along their orbits, their apparent areas change, causing altering their brightness out of eclipses.

The final category is the *W Ursae Majoris* type. As mentioned, it also has a curved maximum brightness. These are typically close binary stars that strongly influence each other. Both the primary and secondary minima are nearly identical, and the overall changes in brightness are relatively small. The systems are contact binary systems, with mass transfer or common envelope occurring. W UMa binaries usually have comparable temperatures in both components and, consequently, very similar minima. Due to strong tidal forces, this type almost always has circular orbits (Percy, 2007).

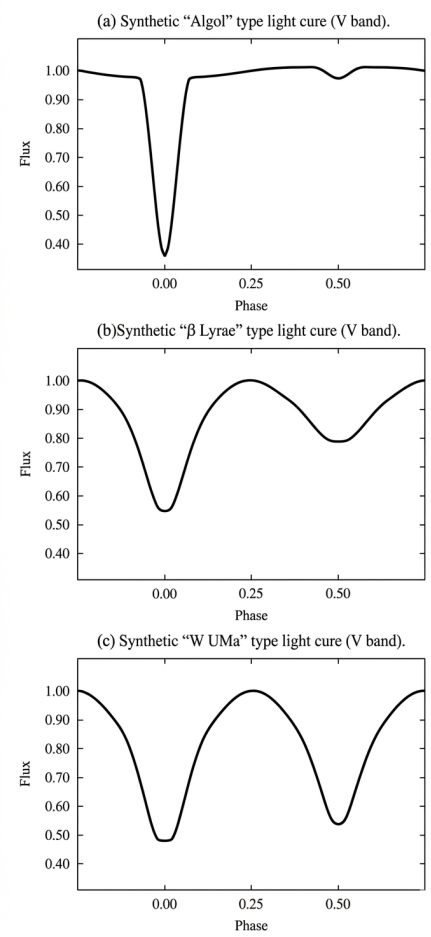

Figure 1.4: Classification of binary stars based on light curves. Taken from Frigo and Giordani (2003).

The classification used so far has been purely phenomenological, based on the shape of the light curve. Although it would be possible to derive some physical conclusions, that is not the purpose of this classification. If we want to understand the actual physical evolution and stage of the system, we must examine the stars from the perspective of the Roche model, which is used to mathematically describe the force field between the components of the system.

The model shows that the potential at any point in the system is given by the gravitational force of each component and the centrifugal force caused by rotation around the center of mass with angular velocity ω:

$$\Phi_R = -\frac{GM_1}{r_1} - \frac{GM_2}{r_2} - \frac{1}{2}\omega(x^2+y^2). \tag{1.4}$$

The masses of the binary components and their orbital motion dictate the distribution of the total potential, which in turn defines the shape of the Roche lobes. To maintain hydrostatic equilibrium, the stars must physically conform to this field, ensuring their surfaces coincide precisely with the equipotential surfaces.

In any two-body system, there are five points where the resultant potential is zero and, therefore, no force acts. One of these so-called Lagrange points is very important for binary star systems. Point L_1 lies on the line connecting the centers of the stars and thus divides two equipotential surfaces. These two separate surfaces are called Roche lobes and define the maximum volume that a star can occupy.

To calculate the size of Roche lobes, one can use an equation that includes only the mass ratio $q = M_2/M_1$:

$$R_L = \frac{0.49 \cdot q^{2/3}}{0.6 \cdot q^{2/3} + \ln(1 + q^{1/3})}. \tag{1.5}$$

This relatively simple equation was derived by Eggleton (1983) and remains a very good approximation to this day. This calculation yields an effective radius, since the actual shape of the lobes is elongated toward the L_1 point and is therefore approximated by a sphere of equal volume.

This equation is important for the physical classification of stars, depending on how far they fill their Roche lobes (Figure 1.5). If the radius of both stars is smaller than the Roche lobes ($R < R_L$), we refer to them as *detached* binaries. The stars are usually far apart and spherical. Most eccentric binaries fall into this category because the tidal forces are so weak that they have not been able to circularize the orbits.

During its evolution, a star may begin to expand until it reaches a critical limit where its radius equals the size of the lobe ($R = R_L$). In this configuration of *semi-detached* binaries, tidal forces begin to play a significant role, and mass transfer to the other star may occur.

The final category consists of *contact* or *over-contact* binaries. Both Roche lobes are filled, and the stars can share a common atmosphere. There could be a massive transfer of mass through the L_1 point and therefore the stars can have similar surface temperatures (Hilditch, 2001).

1.4 Eccentric binary stars

As already mentioned, binary star systems are very important objects in stellar astrophysics. Most binary stars orbit around a common center of mass in circular trajectories, because tidal forces cause the orbits to circularize. However, a non-negligible percentage of systems have non-zero orbital eccentricity e, so-called eccentric binaries (Mazeh, 2008). By observing and studying eccentric binaries, we obtain useful information about the dynamics and evolution of stars and stellar systems. These objects provide valuable insight into the research of tidal interactions, changes in angular momentum, or apsidal rotation. Apsidal motion is affected by the distribution of mass in stars, so it's useful for studying and testing internal structure and relativity (Claret and Gimenez, 2010).

In 1609 and 1619, German astronomer Johannes Kepler published his laws on the motion of planets in the solar system. He was the first to come up with the idea and mathematical solution of ellipses as the trajectories of planets, with the Sun located at one of the foci. Over time, it was discovered that celestial bodies in a gravitational field move along all conic sections. The type of curve along which the body moves depends on the total mechanical energy of the system E:

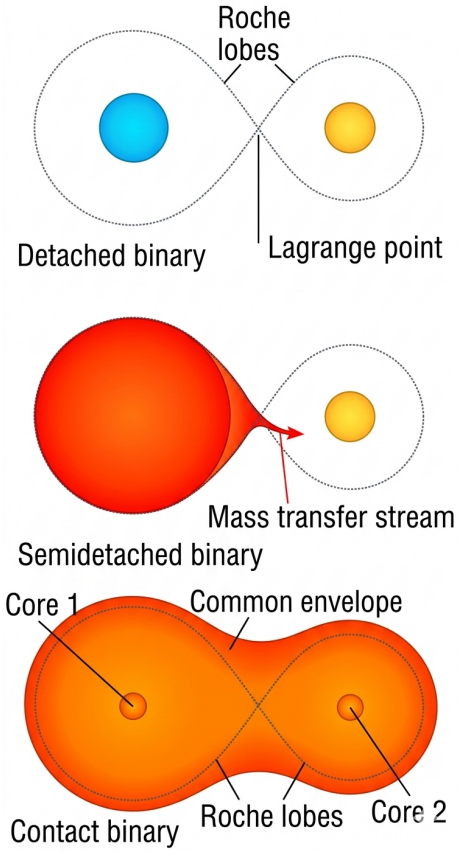

Figure 1.5: Classification of binary stars based on Roche lobe filling. Taken from: onwardtotheedge.wordpress.com.

$$E = T + V = \frac{1}{2}\mu v^2 - \frac{Gm_1m_2}{r}, \tag{1.6}$$

where T is kinematic energy, V is potencial energy, μ is reduced mass, v is relative velocity of the components and r is distance of two objects with m_1, m_2 masses. In the case of negative system energy, bodies move along elliptical trajectories. If the energy is exactly zero, the trajectory will be a parabola. Positive energy means a hyperbolic trajectory (Goldstein et al., 2001). The energy is closely related to the eccentricity of the trajectories, but not explicitly. Eccentricity is a measure of the distribution of energy in the system with respect to the angular momentum L:

$$e = \sqrt{1 + \frac{2EL^2}{\mu k}}, \tag{1.7}$$

where $k = G(m_1 + m_2)$ is gravitational parameter. From relation 1.7, it follows that eccentricity affects the shape of the trajectory of cosmic objects. According to energy, eccentricity will take on the following values:

$$\begin{aligned} E < 0 &\Rightarrow 0 \leq e < 1 \quad \text{(eliptic orbit)} \\ E = 0 &\Rightarrow e = 1 \quad \text{(parabolic trajectory)} \\ E > 0 &\Rightarrow e > 1 \quad \text{(hyperbolic trajectory)} \end{aligned} \tag{1.8}$$

Binary stars are gravitationally bound objects and therefore represent the first case where eccentricity takes values from 0 to 1. The special case $e = 0$ indicates perfectly circular orbits. In Figure 1.6, we can see how the value of e affects the shape of the orbit.

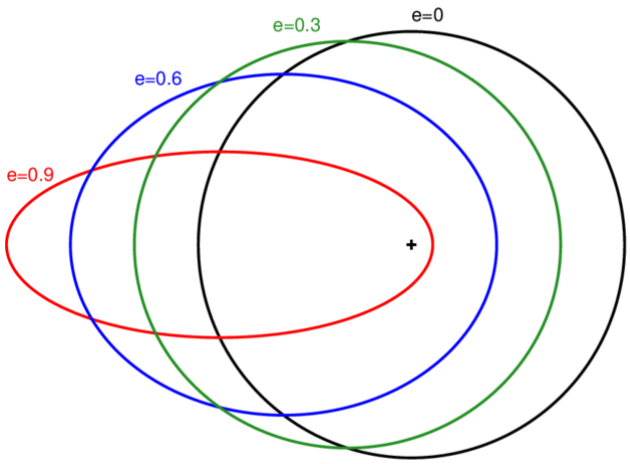

Figure 1.6: The effect of eccentricity on the shape of the orbit. The black plus sign is the center of gravity (Wright and Gaudi, 2012).

Another view of eccentricity is from a geometric perspective. It is the ratio between the semi-major axis (a) and the linear eccentricity (c) that is the distance between the center of the ellipse and the focus :

$$e = \frac{c}{a} = \frac{\sqrt{a^2 - b^2}}{a}, \tag{1.9}$$

where b is semi-minor axis.

However, in astronomy, the semi-major axis and eccentricity more often refer to two points called apses. These are the closest and furthest points from the focus (center of gravity) on an ellipse. The points are called the apocenter and pericenter and are connected by a straight line called the apsidal line or line of apsides. The distance from the center of gravity of the system can be calculated from the following equations:

$$r_{\text{apo}} = a(1 + e), \tag{1.10}$$

$$r_{\text{per}} = a(1 - e). \tag{1.11}$$

Each component has its own apsis points. Both apocenters are connected by a straight line through the barycenter. The same applies to pericenters. In every ideal isolated

system where a spherically symmetric central force (inverse-square) acts, energy and angular momentum are conserved, so particles orbit in ellipses. In a gravitational field, the orientation of the apsidal line is fixed in an ellipse. This fact is based on the existence and conservation of the Laplace-Runge-Lenz vector (LRL). This vector $(\vec{A})$ determines the orientation of the semi-major axis in the direction of the pericenter. In addition to angular momentum, it is determined by the momentum and position vector of the body:

$$\mathbf{A} = \mathbf{p} \times \mathbf{L} - \mu k \hat{\mathbf{r}}, \tag{1.12}$$

where $\hat{\mathbf{r}}$ is unit vector, $\mathbf{p}$ is momentum and $\mathbf{L}$ is angular momentum. The LRL vector is a constant of motion, which means that it is conserved over time and its total derivative of time is zero (Goldstein et al., 2001).

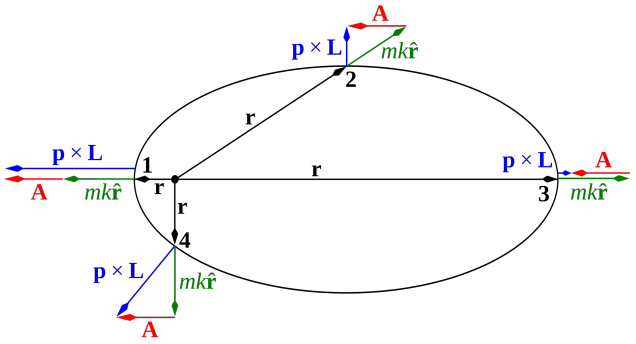

Figure 1.7: The LRL vector maintains the same direction at every point along the trajectory. (from physics.stackexchange.com)

The consequence of conserving the LRL vector in an ideal system is the time invariance of the argument of periastron ω. The line of apsides remains fixed and does not precess. However, these properties will not apply in a general gravitational field, because the force is not exactly inverse-squared. In binary star systems, various interactions affect the behavior of the system as a whole. Due to tidal and rotational deformations or as a result of the gravitational interaction of a third body and the contribution of general relativity, the conservation of the LRL vector is disrupted, and it begins to change direction:

$$\frac{\mathrm{d}\mathbf{A}}{\mathrm{d}t} \neq \mathbf{0}. \tag{1.13}$$

This also causes a change in the argument of periastron and precession of the entire orbital plane. This phenomenon is known as apsidal motion or apsidal rotation (Kopal, 1959).

After one period, the body will not return to the exact same position from a geometric point of view. This will appear as a shift in the position of the periastron, and the change in the argument of the periastron will accumulate:

$$\dot{\omega} = \frac{\mathrm{d}\omega}{\mathrm{d}t}. \tag{1.14}$$

This relationship can be understood as the speed of apsidal motion. Several factors contribute to these changes. The contributions from the aforementioned tidal and rotational

forces, as well as the relativistic correction, can be added together to give the total speed (Claret and Gimenez, 2010):

$$\dot{\omega}_{\mathrm{tot}} = \dot{\omega}_{\mathrm{tid}} + \dot{\omega}_{\mathrm{rot}} + \dot{\omega}_{\mathrm{GR}}. \tag{1.15}$$

In a general relativity, the movement field is understood differently than Newton described it. Unlike the general central force, according to the general theory of relativity (GTR), bodies move under the influence of curved space-time, which is curved by matter. Correction terms are added to the potential, which deflect the body from the precise Keplerian orbit. This is exemplified by the relativistic $\dot{\omega}_{\mathrm{GR}}$ term in equation 1.15. This term in the equation does not depend on the internal structure of stars. It is particularly significant in very massive binaries.

All stars rotate around their axis, and binary stars are no exception. Since they are not solid bodies but are composed of plasma and gas, they form a rotating ellipsoid shape due to centrifugal force. The deviation from a spherical shape causes a non-zero quadrupole moment in the gravitational field. Its value increases with the angular velocity at which the star rotates. The velocity and thus also $\dot{\omega}_{\mathrm{rot}}$ are sensitive to synchronization with orbital motion. In many binary stars, the components rotate at the same speed as they orbit. However, in eccentric binaries, this is generally not the case. $\dot{\omega}_{\mathrm{rot}}$ is an important component of apsidal motion, especially for systems without rotational synchronization.

Tidal forces arise between two or more large bodies under the influence of gravity. In sufficiently large bodies such as planets and stars, a differential gravitational field arises from the mutual interaction of the components of the system. This leads to deformation of the bodies and uneven distribution of mass. Double stars are characterized by protrusions in the direction of the second star. Such a spherically asymmetrical star disrupts the central gravitational field and creates a quadrupole moment. In eccentric systems, it is common for tidal forces not to have the same effect throughout the entire orbit, due to the mutual distance between the components. Because of this, in eccentric systems, the tidal contribution $\dot{\omega}_{\mathrm{tid}}$ of apsidal motion is more significant than others. In circular systems with fast-rotating stars, the $\dot{\omega}_{\mathrm{rot}}$ becomes comparable (Claret, 2004).

The tidal and rotational contributions to apsidal motion are mathematically very similar and are referred to as members of classical theory with the common designation $\dot{\omega}_{\mathrm{cl}}$. They depend on the size of the star and the system as well as on the internal structure of the stars:

$$\dot{\omega}_{\mathrm{cl}} = \dot{\omega}_{\mathrm{tid}} + \dot{\omega}_{\mathrm{rot}} \sim k_2 \left(\frac{R}{a}\right)^5. \tag{1.16}$$

The value of the $\dot{\omega}_{\mathrm{cl}}$ contribution depends on how stars respond to deformation caused by internal and external forces. The distribution of mass inside stars plays a major role here. This information can be provided by the internal structure constant k_2. It is a non-dimensional quantity that determines the concentration of mass in a star. For stars with a very dense core and a sparse atmosphere, k_2 is very small. The value increases as the mass is more evenly distributed, and thus it would reach its maximum value in a homogeneous body.

1.5 Light curves

In the study of variable stars, time dependences in quantities are observed. Such a dependence is, for example, the light curve or, in other words, the dependence of the luminosity of a star on time. For stars that change luminosity periodically, we can convert this time dependence into a so-called *phase function* ϑ, which can reveal different contexts and parameters than the light curve itself. Phase function is the sum of two functions: the *epoch* E and the *phase* φ

$$\vartheta(t) = \frac{t - M_0}{P} = E(t) + \varphi(t), \tag{1.17}$$

where t is the actual time of observation and M_0 is an initial moment and

$$E(t) = \text{floor}(\vartheta(t)); \quad \varphi(t) = \text{frac}(\vartheta(t)). \tag{1.18}$$

The *floor* function will always round down to the nearest integer of the ϑ value. It is then a non-decreasing function that always increments by 1 after each period P. In contrast, the *frac* takes only decimal parts and it is a periodic function. Using the calculated *phase* φ, defined as:

$$\varphi = \text{frac}(\vartheta) = \text{frac}\frac{t - M_0}{P}, \tag{1.19}$$

one can construct a *phase curve*, which graphically represents the data as a function of its phase. Phase takes values from 0 to 1. It shows us changes during one cycle of the periodic event. It can serve us, among other things, to recognize the types of variable stars, for example, if they are pulsating stars, eclipsing binaries (EBs), or some others. EBs are further subdivided according to phase curves (Chapter 1.3).

1.6 *O-C* diagrams

The *O-C* (Observed minus Calculated) diagram is a basic tool for the period analysis and temporal stability of variable stars, especially eclipsing binaries. It requires knowledge of the basic ephemerides (especially the period) of the object, from which we can predict the moments of luminosity minimum (primary or secondary). These calculated predictions (C) can be compared with the actual observed times (O). The difference between the observed time (O) and the calculated time (C) is then plotted as a function of the order of the minimum or of time, which is called *O-C* diagram.

We assume that the function C increases linearly in the form:

$$C = M_0 + PE. \tag{1.20}$$

For each observed minimum time $O(E)$, we then define the difference

$$(O - C)(E) = O(E) - C(E). \tag{1.21}$$

1.6.1 *O-C* diagram patterns

By examining *O-C* diagrams and their patterns, we can determine information about the stability and dynamics of the system (Sterken, 2005):

- **Incorrectly determined period** : An easily recognizable phenomenon that appears as points ordered along a straight line with a non-zero slope.
- **Change in period**: If the points form a parabola or part of a parabola, it means that the period of the system changes over time.
- **Light-time effect**: LiTE indicates the presence of another body in the system. The observed binary system orbits around the center of gravity of a triple (or multiple) system, causing periodic variations in the arrival of light to the observer.
- **Rapid discontinuities**: Sharp changes in the plots may indicate sudden changes in the dynamics of the system, such as rearrangement of the stellar structure or rapid mass transfer.

There are two main patterns that appear in eccentric systems:

- **Eliptic trajectory**: It is typical for eccentric systems that the secondary eclipse does not occur exactly in the middle of the period ($\varphi = 0.5$). This is reflected in the graph by the separation of primary and secondary minima in the vertical direction.
- **Apsidal motion**: The rotation of the periastron causes the points in the graph to form a sinusoidal shape, while the primaries and secondaries remain separate and, therefore, have opposite phases.

The images 1.8 - 1.12 are from "VarAstro" (Sekce proměnných hvězd a exoplanet ČAS, 2023) and show some of the patterns described above.

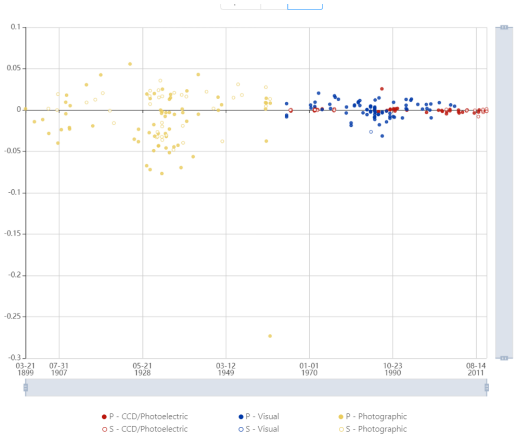

Figure 1.8: VZ CVn: Correctly determined ephemerides, system without changes and evolution.

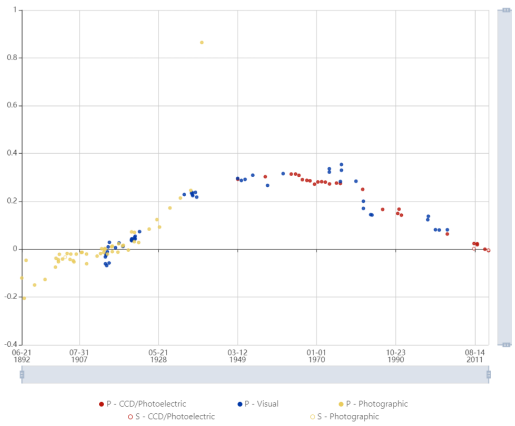

Figure 1.9: RS CVn: Period change.

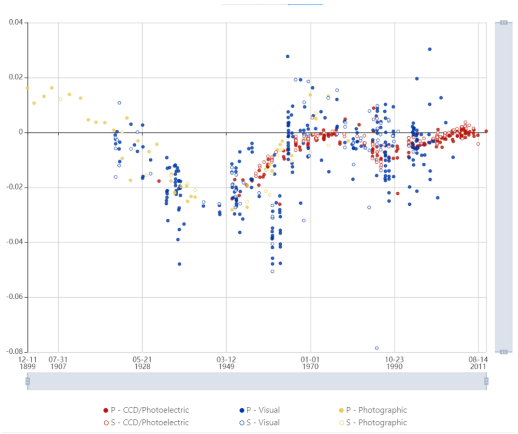

Figure 1.10: AK Her: Third body in system.

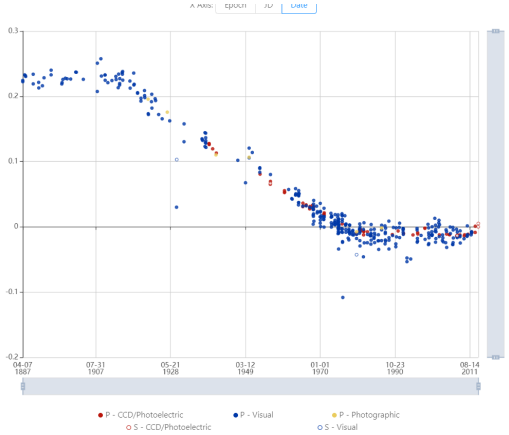

Figure 1.11: R CMa: Rapid change in system

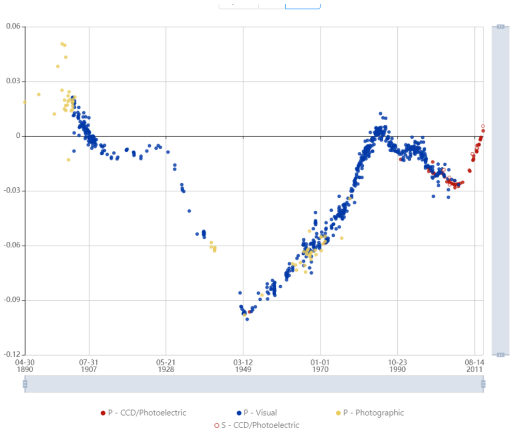

Figure 1.12: Z Dra: A combination of several factors.

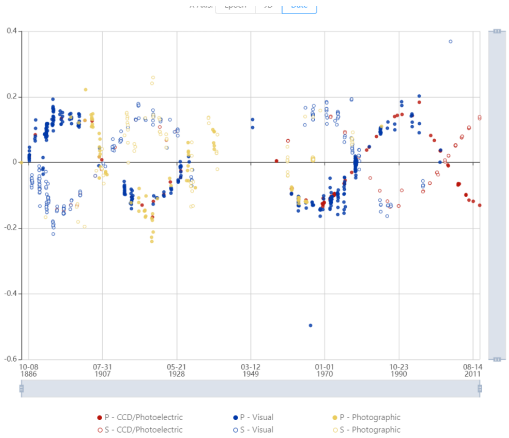

Figure 1.13: Y Cyg: Apsidal motion.

Chapter 2

Data

2.1 Photometry

Observational astrophysics uses several methods to obtain information about space objects. Almost all of them detect electromagnetic waves coming to us from space. The difference between the methods lies in the spectrum they focus on and the signal processing procedure. Photometry is one of the basic and oldest observational methods, but it is very important in modern astrophysics. This method focuses on the integral measurement of photon flux.

The method of photometry dates back to the second century BC. Hipparchus classified several stars according to their brightness. The scale is logarithmic because the human eye also perceives light signals logarithmically according to Weber-Fechner's law. Although magnitudes are a more natural unit of brightness for humans, in photometry we measure luminous flux F physically. This is the amount of energy that passes through a unit area in a given time ($\mathrm{W.m^{-2}}$). According to Hipparchus's scale, when brightness increases by five magnitudes m, the luminous flux increases 100 times. The relationship between these two quantities was mathematically formulated by N. R. Pogson in the 19th century:

$$m_1 - m_2 = -2.5 \log \frac{F_1}{F_2}. \tag{2.1}$$

From the relationship, we can see that in order to perform the calculation, we need to know data about another star with which we can compare the values (Budding and Demircan, 2007).

The brightness of a star is not the same across the whole light spectrum. Each body emits a specific spectrum, which is continuous and depends mainly on its surface temperature. Since this spectrum normally spans a wide range of wavelengths and each detector has a different sensitivity to different wavelengths, photometric filters began to be used in astronomy. The first *UBV* filter system was introduced by Johnson and Morgan (1953). Later, two more filters, *R* and *I*, were added. Each filter has its own specific bandwidth in which it transmits light and filters out other wavelengths. The *V* filter was designed to best match the sensitivity of the human eye. This made it possible to better reproduce old visual observations. With the introduction of photometric systems, observations from different telescopes and observatories could be compared. The *UBVRI* system is still in use today, but with the advent of modern technologies, its shortcomings have become apparent.

Therefore, new filter systems have commonly begun to be used. More than 200 different systems are in use (Fiorucci and Munari, 2003). The most widely used is probably *SDSS* (also known as *ugriz*), which has minimal overlap among its bands and is optimized for modern telescopes and detectors (Fukugita et al., 1996).

As already mentioned, the first photometric detector was the human eye. It was also the only detector until the 19th century, when photographic emulsion plates began to be used. This was a very inefficient method, as only about 5% of photons were captured. Nevertheless, it was the first possibility for objective light capture with longer exposure. Accuracy and efficiency increased with the discovery of the photoelectric effect and the subsequent invention of photomultipliers. These devices were capable of linearly converting photon flux into electric current. However, a major disadvantage was that the photomultiplier could only observe one star at a time.

A revolution in space observation and photometry came in the 1970s with the invention of CCD (Charged-Coupled Device) detectors. These semiconductor chips can record a two-dimensional image of the night sky while having higher quantum efficiency and have gradually become more accurate than photomultipliers. Modern CCD detectors can capture up to 90% of incoming photons. The combination of area and efficiency has increased the detection range of telescopes several times over (Howell, 2006).

From a physical point of view, CCDs function similarly to photomultipliers, as both utilize the principle of the internal photoelectric effect. The difference lies in the design of the individual devices. Silicon is usually used as a semiconductor in CCDs. When a photon with sufficient energy strikes the silicon crystal lattice, it knocks an electron out of an atom. The number of electrons is linearly proportional to the number of photons. Excited electrons are captured in potential wells (pixels) created by voltage on the chip surface throughout the exposure period. After measurement, the signal is transferred to the output amplifier and analog-to-digital converter.

Although CCD detectors are very accurate and efficient, they have limitations. For the photoelectric effect to happen, sufficient energy is needed to overcome the bandgap. At room temperature, photons with a wavelength of less than 1100 nm have sufficient energy (Chromey, 2010).

Nowadays, however, the industry has largely transitioned from CCD to CMOS (Complementary Metal-Oxide-Semiconductor). CMOS sensors operate on the same principle of converting photons into electrical current. The difference, though, lies in the sensor's design. CMOS sensors have an integrated ADC and amplifier in every pixel. A major advantage over CCDs is the absence of blooming, as well as the ability to measure all stars in the image.

Three types of images are used in post-processing: dark frame, bias frame, and flat field. A *dark frame* is used to remove the consequence of dark current because electrons are released even without incident photons. This occurs due to thermal excitation, which can be partially eliminated by lowering the temperature, but a dark frame is required for complete elimination. They are made with the shutter closed and at the same temperature as the specific frame. Another type of noise present in photometry is called readout noise. This is electronic noise caused by the conversion of the signal into digital form. It can be removed by taking *bias frames* with an exposure close to zero and a closed shutter. However, it is no longer as necessary today, since the camera's software can remove noise

directly. Unlike the first two reduction images, *flat field* removes hardware imperfections across the entire measuring device. Each pixel has a different sensitivity from the factory. At the same time, impurities on the optical system and chip may cause diffraction. It must also be taken into account that every optical system suffers from vignetting, i.e., darkening of the image towards the edges. To eliminate these multiplicative problems, an evenly lit area must be photographed. A flat field is usually taken just during twilights or from inside an illuminated dome (Chromey, 2010).

2.2 Sources

Data analysis is one of the most important fields in astrophysics. There are various methods for acquiring data. Each object in the universe requires a different method, depending on the signal received and its form. For the study of variable stars, photometry (2.1) is an important method, and it was the primary source for this thesis. There are two ways to obtain photometric data: to collect one's own data, which allows complete control over the observation and processing, but is very time-consuming; or to obtain publicly available data from a survey, whether from other observers or large observatories and satellites. The majority of the information used here comes from the TESS satellite database, supplemented by data from the ASAS-SN survey and a few of our own observations. Spectroscopy is also important because it provides information about other stellar parameters; however, it was not possible to include this method in the study. During the study, no publicly available data on the investigated objects existed, and the objects were too faint for the author's own observations.

2.2.1 TESS

The Transiting Exoplanet Survey Satellite (TESS) is a space telescope originally designed to search for exoplanets near bright stars; however, it has also been widely used in the field of eclipsing binaries. The entire mission is led by NASA in collaboration with MIT. In 2018, the satellite was launched into a highly eccentric orbit around Earth with a period of 13.7 days.

The project aims to provide a photometric survey in the 600-1000 nm band (red and near-infrared wavelength). Observation of one area of the sky is called a sector and lasts 27.4 days (2×13.7). The area of the sector is observed by four CCD cameras with a total field of view of $24° \times 96°$. TESS is a valuable source of data for binary stars, mainly due to its high-cadence photometry (exposure times of 2-30 minutes), which allows the observation of even rapid brightness changes. And since it observes a single section of the sky for a long period of time, it continuously records many objects at once. The disadvantage of this satellite is its low resolution of 21"/px, which can cause false signals and contamination from surrounding objects (Ricker et al., 2015).

As of April 18, 2026, TESS had confirmed 882 exoplanets and identified another 7,927 candidates (NASA). Furthermore, it discovered more than 10,000 multiple-star systems in 103 surveyed sectors (MUST).

Tables 2.1 - 2.5 present information on the TESS measurements that were available and processed for the purposes of this study.

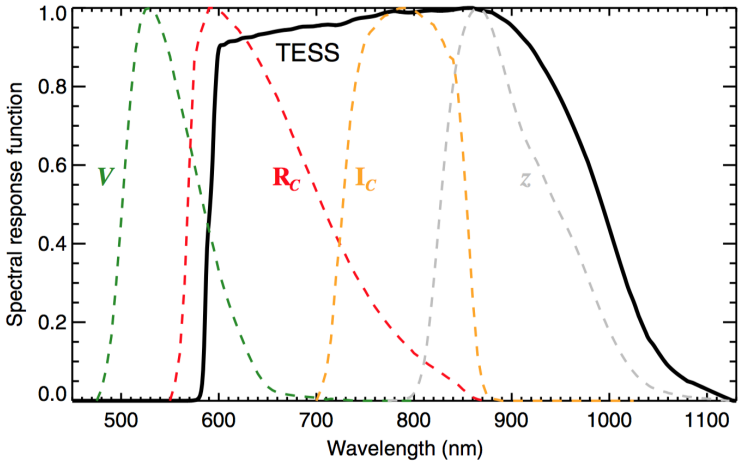

Figure 2.1: TESS wavelength bandpass (Ricker et al., 2015).

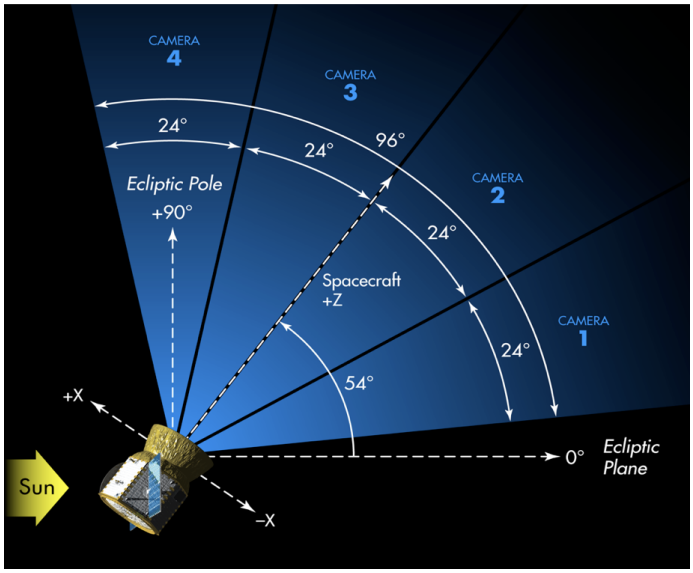

Figure 2.2: TESS camera coverage of the sector (NASA HEASARC).

2.2.2 ASAS-SN

There are many ground-based surveys, but none of the others contained data on the necessary objects except for ASAS-SN. Therefore, it was used as one of the main data sources. All-Sky Automated Survey for SuperNovae (ASAS-SN) is a ground-based photometric survey focused on systematic observations of the entire sky. The project began in 2013, focused on finding bright supernovae, and was run by The Ohio State University. ASAS-SN has its observation network spread all over the Earth, which makes it possible to monitor the entire sky. The network consists of several stations equipped with automatic 14 cm telescopes that have $4.5° \times 4.5°$ the field of view, which in some cases can reach a limiting

Sector	Exposure (s)	Year
8	1426	2019
34	475	2021
35	475	2021
61	158	2023
88	158	2023

Table 2.1: Available TESS sectors for the star 2MASS J08453462 -2158013

Sector	Exposure (s)	Year
9	1426	2019
10	1426	2019
36	475	2021
37	475	2021
63	158	2023
64	158	2023
90	158	2025

Table 2.2: Available TESS sectors for the star 2MASS J10024347 -5643283

Sector	Exposure (s)	Year
6	1426	2018
32	475	2020
33	475	2020
87	158	2024

Table 2.3: Available TESS sectors for the star AT Lep

Sector	Exposure (s)	Year
6	1426	2018
33	475	2020
87	158	2024

Table 2.4: Available TESS sectors for the star CF Mon

18.5 mag. The observation proceeds mainly in two photometric bands, V (Johnson) and g (SDSS), and the signal is captured by CCD cameras (Kochanek et al., 2017).

2.3 Selected objects

As the title of this thesis suggests, the main area of research is eccentric eclipsing binaries. The aim is to process data and search for parameters of specific selected systems. An important criterion was that the system should have an elliptical orbit or at least be a candidate with such a trajectory. Five objects were selected from the work of Kim et al. (2018), which had not yet been sufficiently researched in depth or had not yet been researched at all. The basic information that was known about the objects is presented in table 2.6, and light curves of the objects are plotted in the Figures 2.3 - 2.7.

Period and the position of the secondary minimum on the phase curve are very important parameters for binary stars. Generally speaking, the longer the orbital period of a system, the more time is required to study it. Systems with longer periods typically exhibit a longer period evolution. Moreover, there are fewer timings of brightness minima available, which are important for the study of binary stars. The phase of the secondary minima is equivalent to the system's eccentricity. It indicates the moment when the secondary minimum occurs when converting time to a phase curve (1.5). For systems with circular orbits, the phase of the secondary minima is always 0.5, because the secondary eclipse always occurs halfway through the orbit. For eccentric binaries, the phase value deviates toward 0 or 1. This depends on the geometry of the orbit and the direction from which the object is observed. The more the phase of the secondary minima deviates from 0.5, the greater the eccentricity is likely to be.

Sector	Exposure (s)	Year
17	1426	2019
18	1426	2019
24	1426	2020
57	158	2022
58	158	2022
77	158	2024
78	158	2024
84	158	2024
85	158	2024

Table 2.5: Available TESS sectors for the star V919 Cep

Name	**RA** [^{h} ^{m} ^{s}]	**Dec** [° ’ ”]	**Period** [d]	M_0	**Phase**	**Mag** (V)
2MASS J10024347 -5643283	10 02 43.47	-56 43 28.29	10.940	52806.140	0.323	12.91
2MASS J08453462 -2158013	08 45 34.62	-21 58 01.34	11.042	54400.444	0.860	12.46
V919 Cep	22 59 40.81	+65 12 40.11	1.852	51295.901	0.492	10.48
AT Lep	05 48 17.06	-25 02 30.73	10.649	52634.787	0.449	11.56
CF Mon	06 49 21.99	-00 23 46.52	2.610	30047.640	0.512	13.20

Table 2.6: Studied objects. The ’Phase’ column indicates at what phase of the period the secondary minimum occurs. For the full format of Julian date 2 400 000 needs to be added to the value M_0.

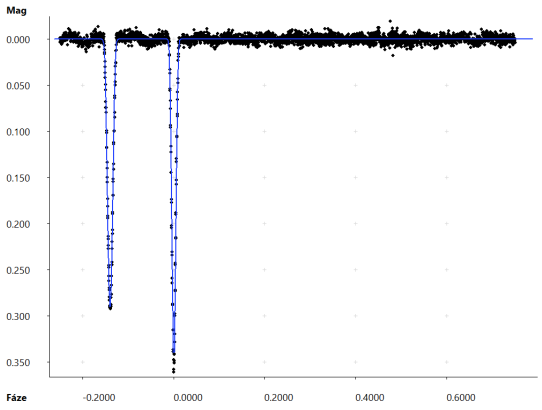

Figure 2.3: Light curve of 2MASS J08453462-2158013 from TESS (sector 34) with phenomenological model from SILICUPS program.

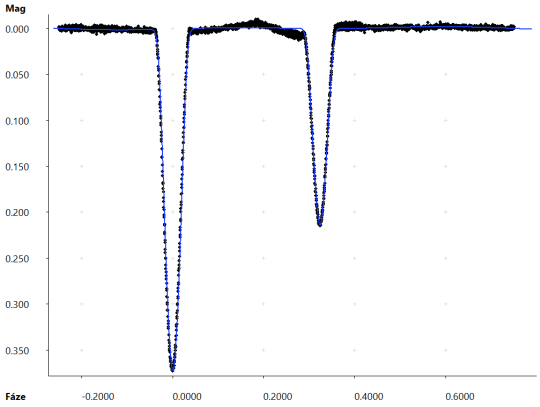

Figure 2.4: Light curve of 2MASS J10024347-5643283 from TESS (sector 37) with phenomenological model from SILICUPS program.

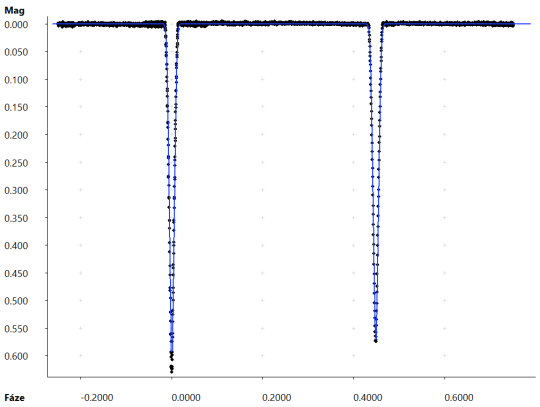

Figure 2.5: Light curve of AT Lep from TESS (sector 33) with phenomenological model from SILICUPS program.

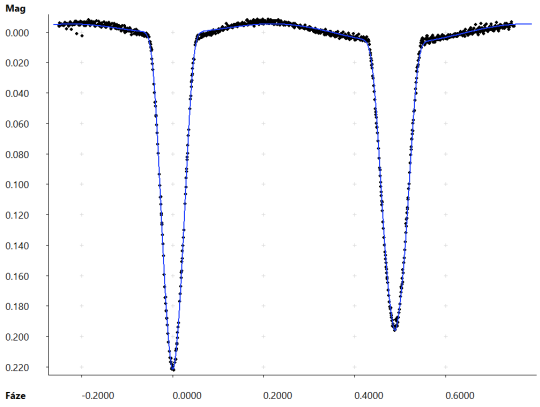

Figure 2.6: Light curve of V919 Cep from TESS (sector 18) with phenomenological model from SILICUPS program.

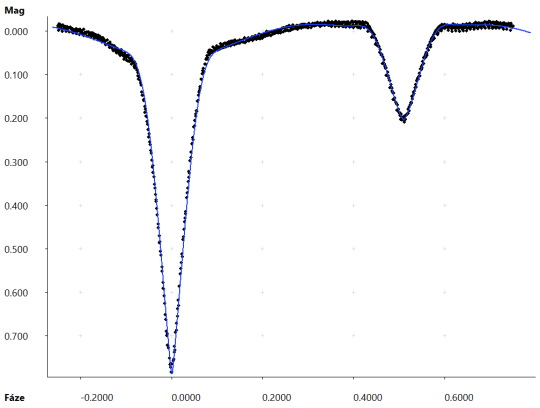

Figure 2.7: Light curve of CF Mon from TESS (sector 6) with phenomenological model from SILICUPS program.

Based on their light curves (Figures 2.3 - 2.7), all of the observed objects can be classified as Algol-type (Watson and AAVSO). The CF Mon and V919 Cep systems do not have a completely constant maximum; nevertheless, the beginning and end of each eclipse can be identified. These non-constant parts could indicate a non-spherical shape of system components caused by tidal forces. Based on the available information from the PHOEBE program, we can conclude that these are detached systems in all cases.

Chapter 3

Data processing

3.1 Used programs

3.1.1 SILICUPS

The Simple Light Curve Processing System (SILICUPS v3.2.4) is a program described by Pejcha et al. (2022), and it is used to process photometric data. It allows users to view time series and convert them into phase curves. In the *Phase curve* tab, you can set and adjust the system's ephemerides. The *Phase curve fit* tab is used to determine the phenomenological model of the phase. Modeling in the program is based on a mathematical description by Mikulášek (2015), which uses orthogonal polynomials and harmonic functions for an accurate analytical description of the light curve.

The program allows the application of the phase curve model to a time series and uses it to determine minima timings that are needed to construct an $O-C$ diagram. If the data are sufficiently accurate, the program can automatically identify all minima and determine whether each represents primary or secondary eclipse. Depending on how well the model fits the curve, it also determines the uncertainty of the timings of minima.

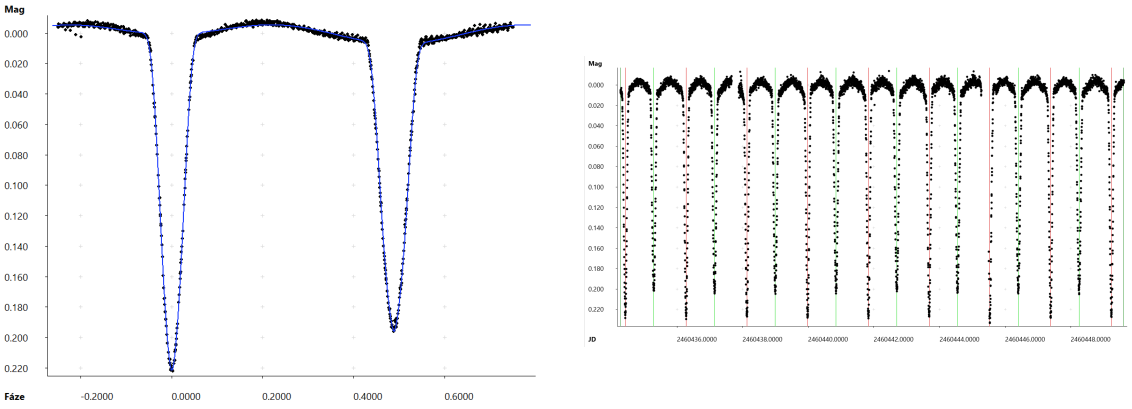

Figure 3.1: A preview from the SILICUPS program. The phase curve with the phenomenological model (left) and the time series with identified minima timings (right) for one TESS sector of the V919 Cep binary star.

3.1.2 PHOEBE

Modeling the light curves of eclipsing binaries is a fundamental part of their study. There are many ways to model a light (or phase) curve. For example, in the Silicups program, these are phenomenological models, which are essentially just functions that best fit the given curve. Such models tell us nothing about what the star actually looks in reality. For these purposes, physical models are used to determine the actual parameters of objects. The PHOEBE v0.32 program (PHysics Of Eclipsing BinariEs) (Prša and Zwitter, 2005) was used for our work. This program is based on the proven Wilson-Devinney code (Wilson and Devinney, 1971), which has already become the standard in this field, although it sometimes struggles with convergence, parameter degeneracy, and sensitivity to initial conditions. PHOEBE retains the basic physical aspects of the WD code, intending to modernize the entire process. The program improves algorithms and adds other robust numerical methods such as Nelder-Mead simplex. Moreover, a user interface has been made to assist users in handling the parameter settings and the model itself.

Modeling light curves in PHOEBE is not a fully automatic process. First, it is necessary to set at least the estimated initial conditions and parameters. The program then uses iterative methods to minimize the difference between the observed and synthetic curves. This minimization is achieved by combining the ”Differential Corrections” method from the original WD code with the more robust Nelder-Mead simplex or heuristic scanning method. Numerical methods such as these are sensitive to initial conditions. They are designed to find the global minimum of a minimum space solution function, but sometimes the method may identify a false minimum, which is only a local minimum.

Model optimization is verified by minimizing the χ^2 statistics, where a lower value indicates a superior fit. Despite the low χ^2 value, the solution may not be optimal. Since this is a physical model rather than a phenomenological one, it is crucial to assess the physical plausibility of the fitted parameters.

The PHOEBE program allows optimization over a wide range of parameters, so it is advisable to check at least some of the available information and parameters that are already known for the initial conditions. The basic parameters for eclipsing systems are mainly the period P, but also the eccentricity e, the inclination i, and the argument of periastron ω. These parameters determine the system's geometry and orientation. Other parameters relate to individual components. The radii of stars are calculated in the program using Roche potentials Ω, which affect the width of the eclipses in the model. Potentials can also affect the shape of the entire curve, as they describe how individual components are deformed by tidal forces or how much they fill Roche lobes. Estimating effective temperatures T_{eff} without spectroscopy is quite difficult, but modern satellites can now determine at least the temperature of the brighter component for large numbers of objects. The less bright component can be estimated from the shape of the curve, based on the depth of the eclipses and whether the system is detached or contact. Furthermore, the radiative properties of the stellar surfaces must be specified. PHOEBE calculates limb darkening using tabulated coefficients that are contingent on temperature and surface gravity. The parameters of reflection (albedo) and gravity brightening further influence the detailed shape of the eclipses and out-of-eclipse variations, especially in semi-detached or contact binaries. If necessary, starspots or a third light can also be added.

It is not possible to determine the masses of the individual components of a binary star from photometric data. Since the program does not allow individual masses to be obtained just from photometry, the only option is to determine the parameter q, i.e., the mass ratio M_2/M_1. The 'q-search' method differs from the method used to calculate other parameters. The light curve does not depend directly on the masses themselves, but on the geometry of the system, which is determined by Roche potentials. Therefore, different combinations of q parameter values and potentials can produce very similar eclipse shapes. To avoid convergence to a local space solution function, q is not fitted as a free parameter. Instead, an interval q is selected (typically 0-2), and all other model parameters are optimized separately for each value of this parameter. The χ^2 is calculated from each iteration. The result of the entire process is the $\chi^2(q_i)$ function, which minimum determines the most probable value of the mass ratio. The resulting q-search graphs for all systems are included in the appendix 4.3.

3.1.3 Python

Python is one of the most globally used programming languages. It has also become one of the fundamental scientific tools. In science, it is used mainly for easy implementation and code experimentation, which enables efficient data processing. This is due to Python's code readability, simple syntax, and ever-growing library ecosystem. Many of these libraries are very useful to scientific communities: SciPy, NumPy, and Pandas (numerical calculations); Matplotlib and Plotly (graphical displays, visualization). Libraries such as Astropy and Lightkurve are designed specifically for astrophysics.

For this research, Python was mainly used to aid in the downloading and processing of data. The *Lightkurve* library Lightkurve Collaboration et al. (2018) is designed for processing light curves and enables direct data download from the TESS satellite, as doc. Ondřej Pejcha presented at the conference about Variable Stars (Pejcha, 2020). The original code was published by NASA. The script searches for the observed area based on the entered coordinates and lists all available sectors where the object is located. Then, the sector to be further processed is determined. The area on the rendered map where the flux will be counted and the background subtracted, is determined based on the aperture mask. Subsequently, another star (non-variable) is defined, according to which the change in luminosity in the examined star is determined. Using Pogson's equation, the flux is converted to magnitudes. Thus, the output of the code is a time series of the magnitude for all available sectors.

Python was also used in this work to detrend light curves, process some data, and plot graphs. Detrending was necessary in some sectors to remove trends in data that were not caused by physical phenomena, but probably by measurement errors and apparatus defects.

For reliable detrending, a function from the NumPy library was used that applies Chebyshev polynomials (numpy.polynomial.Chebyshev.fit). The use of these orthogonal polynomials is more stable in numerical iterations than power series expansions, and they do not introduce unwanted artificial products during processing. The polynomials are set to a degree that best covers the residuals. These residuals are then subtracted from the light curve.

3.1.4 OCFit

Minimum brightness timings in binary stars are crucial information for studying the evolution of the system, as they are necessary for creating an $O-C$ diagram. The OCFit software v.0.2.2 (Gajdoš and Parimucha, 2019) was used to work with this type of data. The program is is written in Python and can be run interactively.

To use OCFit, the user only needs to input the minima times, and the program automatically calculates the $O-C$ values and plots them on a graph. It is necessary to specify basic ephemerides such as the period P and the initial moment M_0. The program can then fit different curves of O-C corresponding to the pattern shown in Chapter 1.6.1.

In addition to a simple linear fit, the program can also model more complex phenomena. A parabolic trend in the case of a change in period or mass flow, or a sine wave indicating a third body in the system. For eccentric binary stars, it is also possible to fit the apsidal motion. The output of the apsidal motion model includes important parameters such as the system's eccentricity, the argument of periastron, or the apsidal motion rate.

Chapter 4

Results

As previously mentioned, only photometric data were available for the objects under study, and therefore, all research and results are based on this data. The primary data source was the TESS satellite, supplemented by the ASAS-SN survey (chapter 2.2) and a few of our own observations. In addition to these two projects, other sources of photometric data were also examined during working on this thesis: SuperWasp (Thiemann et al., 2022), AAVSO (AAVSO, 2024), ATLAS (Tonry et al., 2018), KWS (Maehara, 2014), OMC (Mas-Hesse et al., 2003), ZTF (Bellm et al., 2019), APASS (Henden et al., 2015), PanSTARRS (Chambers et al., 2016), IRSA (NASA/IPAC Infrared Science Archive, 2024), VarAstro (Sekce proměnných hvězd a exoplanet ČAS, 2023). However, for the studied objects, no data were available in these surveys, or the data were not usable for this thesis.

4.1 Physical models

Physical models allow us to determine the values of real stellar and orbital parameters using only light curves. Despite the fact that analysis based solely on photometry is quite limiting, physical models were constructed for all objects, and all possible parameters were obtained. The models were processed in PHOEBE software (chapter 3.1.2). For modelling purposes, individual sectors from TESS were used for accuracy and clarity.

The summary tables also list the distance (d) for all objects. This parameter was taken from the Gaia DR3 catalog (Gaia Collaboration et al., 2023). The tables contain the masses of the M_1 and M_2 components. It was not possible to calculate the individual masses from the physical model due to the absence of spectral measurements. Therefore, M_1 was estimated in a first approximation from the effective temperature of the component (T_{eff}). The method and calibration tables were described by Pecaut and Mamajek (2013), which are focused on main-sequence stars. Subsequently, M_2 was calculated from the mass ratio (q-parameter). This method is more precise than estimating the second mass from the temperature as well. It must always be kept in mind that determining temperatures in this way, without spectra, is only a rough estimate. The uncertainty in the masses was determined to be 15% of each value. The article from which the masses were estimated lists uncertainties of around 10%, but other uncertainties from the determination of q and, in particular, temperatures were also taken into account here.

Furthermore, the temperature of the hotter component was at least approximately known from other catalogs or SEDs. The VO Sed Analyzer (Bayo et al., 2008) service was used to obtain SEDs. The temperature error is actually higher than listed in Tables 4.1 - 4.5, because the listed values are from the PHOEBE program, whereas estimates from SEDs likely have greater uncertainty.

In the physical modelling, it was assumed that both components rotate in synchronization with the orbital period. Such a scenario is typical for binary star systems with circular orbits. It appears that all binary stars tend to circularize their orbits, but some systems did not have enough time for this process. Eccentric binary stars are characterized by so-called pseudo-synchronization.

4.1.1 2MASS J10024347-5643283

Physical model of this system suggests that the system consists of two main-sequence stars. The primary component is slightly smaller and less luminous than the Sun. The secondary component is even smaller. For the modelling, the primary star's temperature was set to 5700 K, but it had to be lowered slightly. The system 2MASS J10024347-5643283 shows no unusual features other than a high eccentricity.

The 4.1 plot clearly shows a noteworthy phenomenon. Although the model fits quite accurately in other parts of the phase φ, there are much larger residuals in the eclipses. This effect does not necessarily mean the model is inaccurate, but it is a mathematical problem. It is caused by a phenomenon known as "slope sensitivity," which typically manifests as a W-shaped curve

$$\Delta mag \approx \frac{\mathrm{d}(mag)}{\mathrm{d}\varphi}\Delta\varphi. \tag{4.1}$$

In very steep parts, the sensitivity of the derivative is much greater than in flat sections outside the eclipse. Thus, even a small phase shift can cause a large deviation in magnitude. At the minimum of the eclipse, the derivative is zero, and therefore the residuals also converge to zero.

Parameter	Value	Error
T_1 [K]	5600	40
T_2 [K]	4820	30
$M_{\mathrm{bol},1}$ [mag]	2.47	0.10
$M_{\mathrm{bol},2}$ [mag]	3.08	0.10
R_1/a	0.13	0.01
R_2/a	0.12	0.01
e	0.287	0.001
q	0.60	0.01
i [°]	83.271	0.001
$M_1[M_\odot]$	0.8	0.1
$M_2[M_\odot]$	0.8	0.1
d [pc]	1572	32

Table 4.1: Parameters from physical model of 2MASS J10024347-5643283.

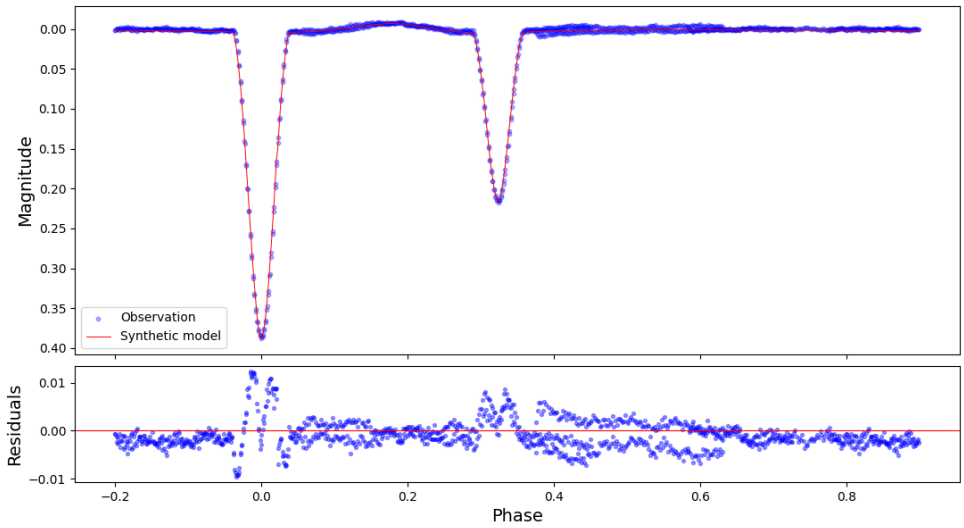

Figure 4.1: 2MASS J10024347-5643283 physical model.

4.1.2 2MASS J08453462-2158013

The 2MASS system is characterized primarily by a very high eccentricity of $e = 0.613$. Although it is not possible to directly determine the system's semi-major axis, the small relative radius suggests that the stars are small or distant relative to each other. Based on their temperatures, the stars are similar to the Sun, so we assume they are main-sequence stars rather than dwarfs. Similarly, the light curve indicates the absence of mass transfer, even during periastron passage. The shape of eclipses suggests that the components are

likely far apart with a large semi-major axis. But the narrow eclipses may also be caused by the high speed at the periastron, due to the system's high eccentricity. The residuals 4.2 show fluctuations that do not originate from the physical properties of the stars, and the signal likely does not belong to the system under study either. It is a remnant of a third light source (Chapter 4.1.2) that could not be removed.

Parameter	Value	Error
T_1 [K]	6520	90
T_2 [K]	5900	80
$M_{\mathrm{bol},1}$ [mag]	3.38	0.10
$M_{\mathrm{bol},2}$ [mag]	3.90	0.10
R_1/a	0.05	0.01
R_2/a	0.05	0.01
e	0.613	0.001
q	0.91	0.01
i [°]	86.140	0.001
$M_1[M_\odot]$	1.3	0.2
$M_2[M_\odot]$	1.2	0.2
d [pc]	580	12

Table 4.2: Parameters from physical model of 2MASS J08453462-2158013.

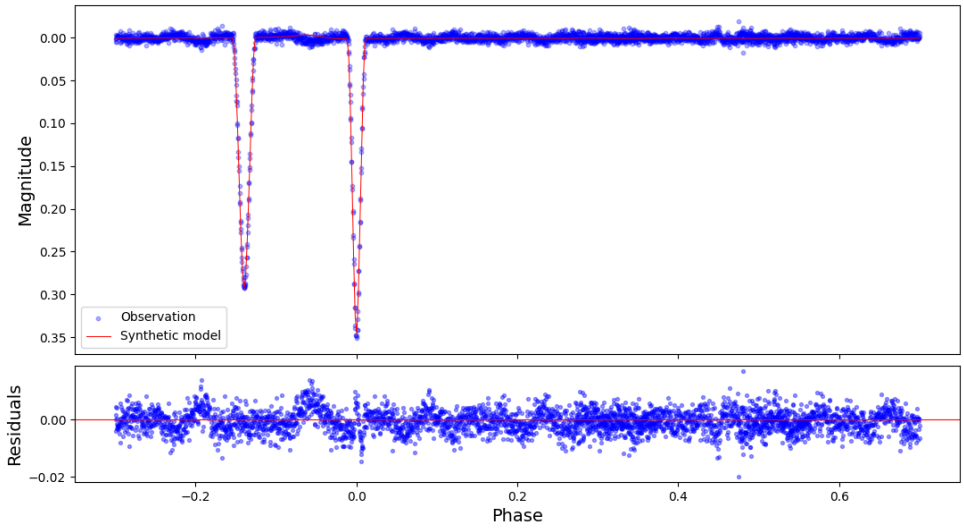

Figure 4.2: 2MASS J08453462-2158013 physical model

During the initial processing of the signal from the 2MASS J08453462-2158013 object, a fluctuation appeared at the object's maximum brightness instead of a constant signal, as shown in Figure 4.3 (left).

It seemed that this might be a sign of pulsations in one of the components. That would make this binary star an interesting and unusual system. However, the poor resolution of the TESS satellite had to be taken into account. Figure 4.4 (left) illustrates how the area from which the signal is read is determined. It can be seen that the star's area is relatively large, which could indicate another, indistinguishable light source. Unfortunately, no photometric data other than TESS data are available for this system, so it was not possible to rule out a possible third light source.

The problem was solved by making a minor adjustment to the script that downloaded and read the data. This was because, while examining other objects in the field, the signal from the binary star was still being read. After the modification and a significant increase in the threshold, it was finally determined that the pulsations originate from the source shown in Figure 4.4 (right). The separated signal is then shown in Figure 4.3 (right), which displays variations with a period of approximately 0.16 days, which would be interesting to investigate in more detail.

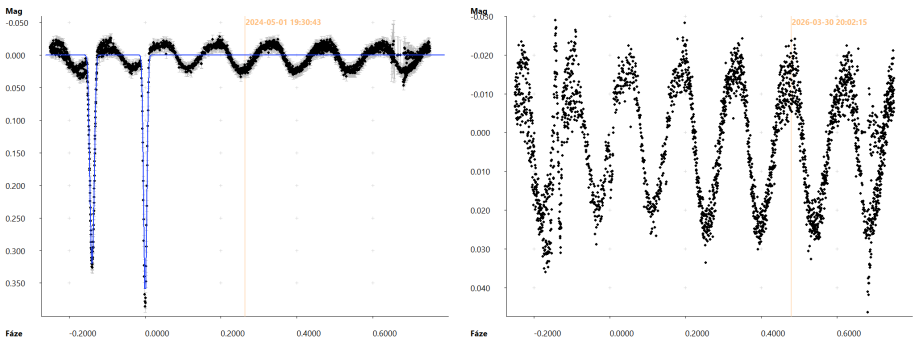

Figure 4.3: Pulsations detected from another source. The original curve is on the left, and the filtered curve of the pulsations is on the right.

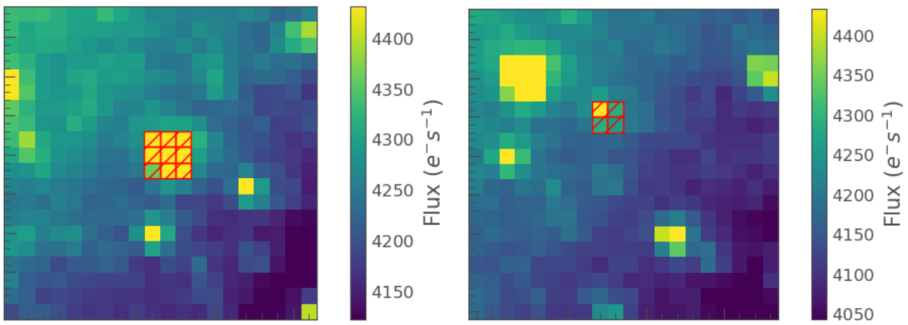

Figure 4.4: The boundary (mask) for selecting the 2MASS J08453462-2158013 object. On the left is a binary star; on the right is the star from which the pulsation signal was infiltrated.

4.1.3 V919 Cep

For physical modelling, it is helpful to have at least some parameters determined in advance. Typically, these parameters include the temperature of the primary component. Assuming this parameter is correctly determined, it should not need to be significantly adjusted during modelling. For the object V919 Cep, catalogs listed various temperatures ranging from 6000 to 12000 K. For modelling purposes, the lower limit of 6000 K was chosen. However, the resulting temperature of the primary component is 11000 K. It can be assumed that the temperature of 12000 K, on which several sources agreed, was a combination of the fluxes of both components. The SED calculation estimated the temperature to be 11350 K using a blackbody model. The resulting values for the V919 Cep parameters are listed in Table 4.3. Assuming components are main-sequence stars, they are very massive and luminous. They fall between spectral classes A and B.

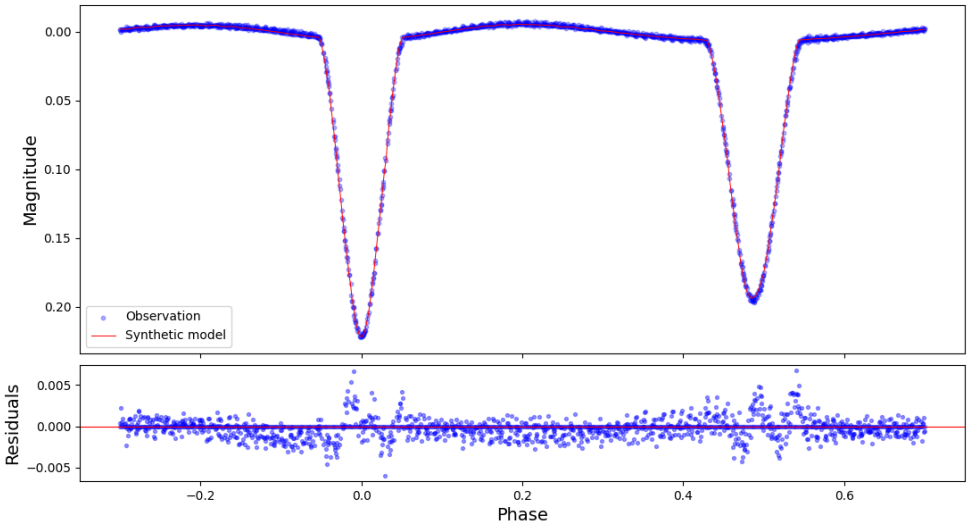

Figure 4.5: V919 Cep physical model.

4.1.4 AT Lep

The Figure 4.6 shows two narrow eclipses and a constant part of the curve outside of them. This could indicate small stars, but Table 4.4 reveals that the stars are similar to each other and have temperatures of around 6200 K. They are therefore Sun-like stars, and the narrow eclipses thus imply a relatively large semi-major axis. This is also confirmed by the small values of the relative radii R/a.

Parameter	Value	Error
T_1 [K]	11000	50
T_2 [K]	10000	50
$M_{\mathrm{bol},1}$ [mag]	0.31	0.10
$M_{\mathrm{bol},2}$ [mag]	1.11	0.10
R_1/a	0.22	0.01
R_2/a	0.18	0.01
e	0.088	0.001
q	0.72	0.01
i [°]	77.779	0.003
$M_1[M_\odot]$	2.5	0.4
$M_2[M_\odot]$	1.8	0.3
d [pc]	845	16

Table 4.3: Parameter from physical model of V919 Cep.

Parameter	Value	Error
T_1 [K]	6200	30
T_2 [K]	6170	30
$M_{\mathrm{bol},1}$ [mag]	3.74	0.10
$M_{\mathrm{bol},2}$ [mag]	4.06	0.10
R_1/a	0.05	0.01
R_2/a	0.05	0.01
e	0.095	0.005
q	0.92	0.01
i [°]	89.45	0.05
M_1 $[M_\odot]$	1.2	0.2
M_2 $[M_\odot]$	1.1	0.2
d [pc]	455	10

Table 4.4: Parameter from physical model of AT Lep.

4.1.5 CF Mon

Even at first glance at the light curve of the star CF Mon, it is noticeable that this is an interesting system. There is a large difference in the depth of the individual eclipses, and there is also no constant brightness outside the eclipses.

CF Mon was difficult to model because it has several unusual aspects. The resulting temperature of the primary component was 9100 K. It was unclear which temperature to use as the input parameter, as some sources reported a temperature of around 6000 K, while others reported around 9000 K. The SED fit revealed a temperature of 10450 K, but this is based purely on photometry. Therefore, the initial temperature of the primary star was set to 9000 K.

As can be seen in the phase diagram and in the residuals, the primary eclipse model differs from the observed data during the descending phase. This is due to the asymmetry

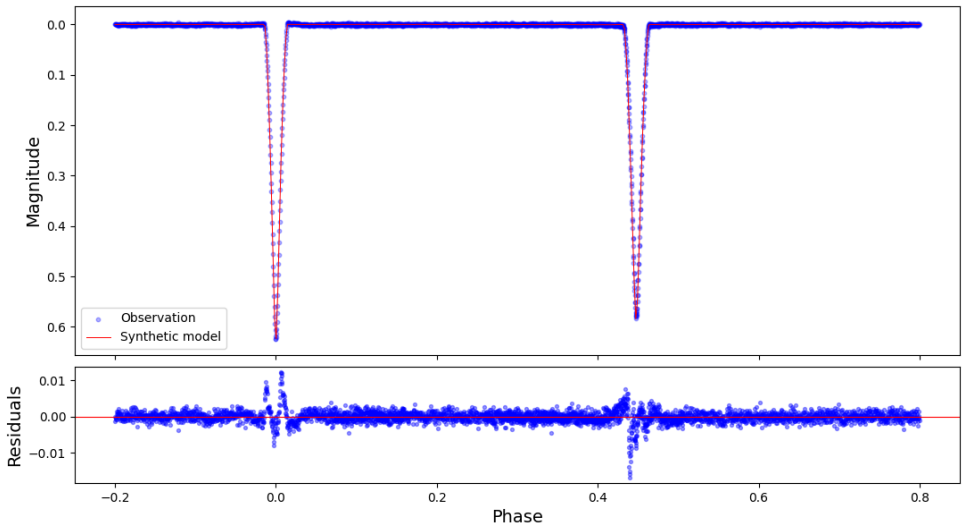

Figure 4.6: AT Lep physical model.

of the eclipse, which could not be adequately fitted. It is unclear why this asymmetry arose. The reason may be a large spot on the star's surface with a different temperature from the rest of the surface. Another possible explanation could be an accretion disk or a flow of matter from one star to the other. The most reasonable explanation, also supported by the fact that the brightness changes even outside the eclipses and increases continuously until the moment of the secondary eclipse, is a phenomenon known as the reflection effect. This occurs when one star is much hotter than the other. The lower-temperature star is strongly heated on its surface at the side facing the hotter star.

Another issue was adjusting the depth of the eclipses. The model consistently tended to show deeper eclipses than they actually are. This suggested the presence of a non-zero third light (L_3), which could indicate another body in the system whose eclipses are not visible, mass transfer, or an accretion disk. However, a more likely theory is a star in the background at a different distance from the studied system, and due to the low resolution of the cameras, it is not possible to distinguish this object.

A key factor complicating the assessment of the system's true nature was the fact that the parameter q, and thus the mass ratio, was greater than 1. This implies that the secondary component should be more massive than the primary one. However, this fact does not align with a comparison of the stars' temperatures. According to the model, the primary star is much hotter than the secondary star. A possible explanation is a system in which at least one component has already evolved and is no longer on the main sequence, and is therefore likely a red giant. Combined with the above-mentioned facts, this system is intriguing but difficult to validate without precise spectroscopic measurements.

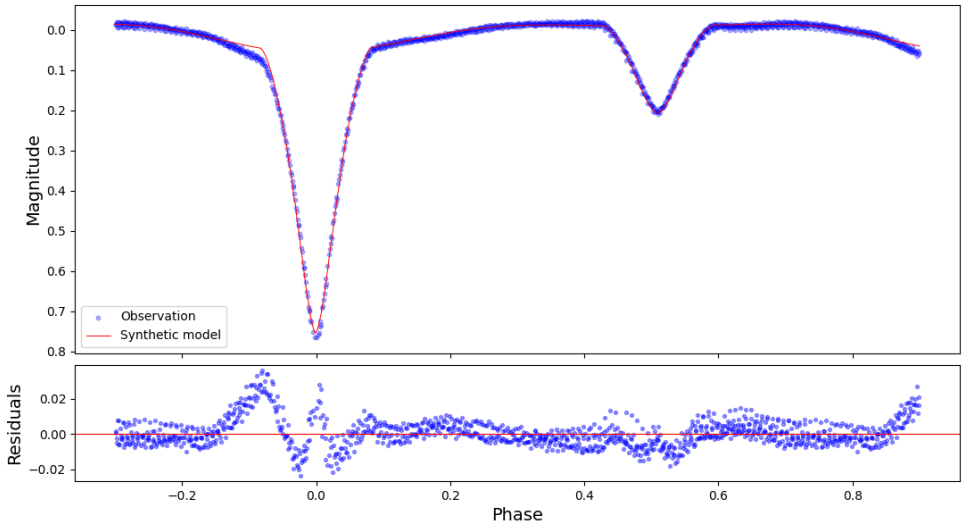

Figure 4.7: CF Mon physical model.

Parameter	Value	Error
T_1 [K]	9100	20
T_2 [K]	3000	90
$M_{\mathrm{bol},1}$ [mag]	-0.33	0.10
$M_{\mathrm{bol},2}$ [mag]	4.26	0.10
R_1/a	0.25	0.01
R_2/a	0.28	0.01
e	0.016	0.001
q	1.52	0.01
i [°]	83.93	0.02
$L_3[\%]$	21	1
$M_1[M_\odot]$	2.2	0.3
$M_2[M_\odot]$	3.3	0.5
d [pc]	4400	300

Table 4.5: Parameters from physical model of CF Mon.

4.2 *O-C* diagrams

$O-C$ diagrams are used to study the long-term evolution of binary star systems (chapter 1.6). The OCFit program (3.1.4) was used to calculate the diagram values. For $O-C$ calculations, it is necessary to derive the timings of brightness minimum. Since two main sources of photometric data were used, each source required a different method for determining the minima timings.

Thanks to the high quality of the TESS data, which consists of long, uninterrupted observations at a high cadence, it was possible to process the data using the SILICUPS program. This program employs a phenomenological phase curve model, which it fits to the time series and automatically determines the times of the minima.

Processing data from ASAS-SN required a different approach, as it was not possible to determine the timings of the minima from the time series alone. This was due to very poor coverage of data points, particularly around the minima during occultations, making it impossible to identify the exact time. Therefore, instead of direct processing in SILICUPS, a Python script provided to me by my consultant, Jakub Kolář was chosen. The minimum times were determined by numerically minimizing the phase shift between the observed data and the theoretical model from the SILICUPS system. The calculation was performed using the algorithm for minimizing the weighted residuals during linear interpolation of the model. The bootstrap statistical method was used to estimate the uncertainty of the determined phase shift, accounting for both measurement errors and the influence of the random distribution of points. The resulting phase shift was then transformed into the times of the primary and secondary minima using the known period and epoch at the midpoint of the observed series. Due to the large dispersion of data, this method was less accurate, as evidenced by the error bars, which are much larger than in the previous method.

As far as possible, the ephemerides (M_0 and P) were fitted and adjusted using $O-C$ diagrams. The adjusted results are listed in the tables with individual stars. A correctly identified M_0 pattern is characterized by the fact that the primary minima lie on the zero line. Any discrepancy between the identified period and the true period will result in a linear trend of the minima.

Object	JD start	JD end	Date start	Date end
2MASS J10024347-5643283	2457666.891	2460775.078	5.10.2016	9.4.2025
2MASS J08453462-2158013	2457529.551	2460739.351	21.5.2016	4.3.2025
V919 Cep	2451295.837	2461108.545	27.4.1999	9.3.2026
AT Lep	2453860.204	2461090.426	4.5.2006	18.2.2026
CF Mon	2455953.948	2460740.298	27.1.2012	5.3.2025

Table 4.6: The time period from which data for individual objects was collected. JD means Julian Date.

4.2.1 2MASS J10024347-5643283

From the perspective of the $O-C$ diagrams, the system is not unusual. It can be seen that both the primary and secondary minima lie on the zero line with small deviations, which,

however, fall within the error bars, apart from a few secondary points, which may have been inaccurately identified but do not distort the final result in any way. Thus, the system is steady-state, and the period has been correctly determined.

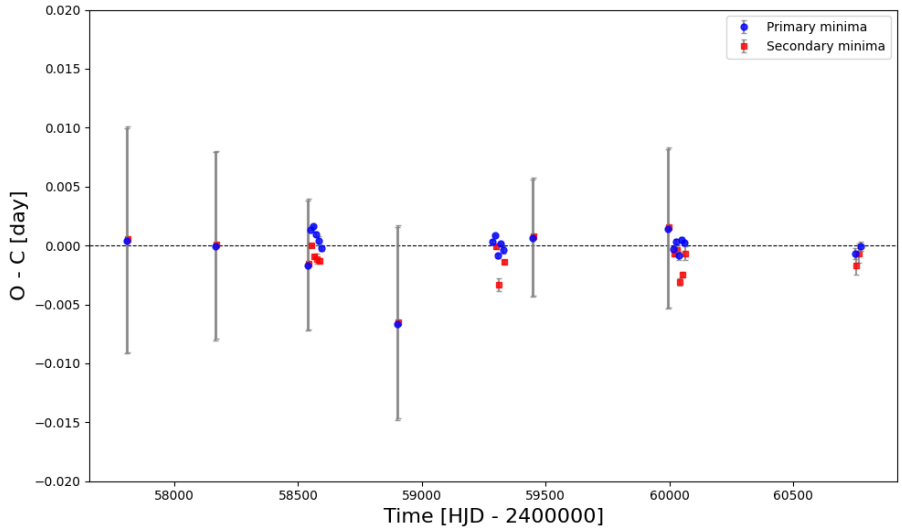

Figure 4.8: 2MASS J10024347-5643283 $O-C$ diagram.

Parameter	Old value	New value
P	10.9400	10.9399(8)
M_0	52806.140	58550.614(2)

Table 4.7: Adjusted ephemerides for 2MASS J10024347-5643283. M_0 is in HJD-2400000.

4.2.2 2MASS J08453462-2158013

It is not entirely clear why the primary and secondary points are mixed up in the 4.9 graph and do not all lie on a single line. One possibility is that the OCFit program incorrectly identified which minimum it was dealing with when calculating the $O-C$ values. However, this is unlikely. Another possibility is that the graph is correct, but the vertical differences between the points are negligible compared to the length of the entire period (11.04 days), so they appear to be inaccurate. Unfortunately, it was not possible to verify these assumptions because the only data source for this object was the TESS satellite.

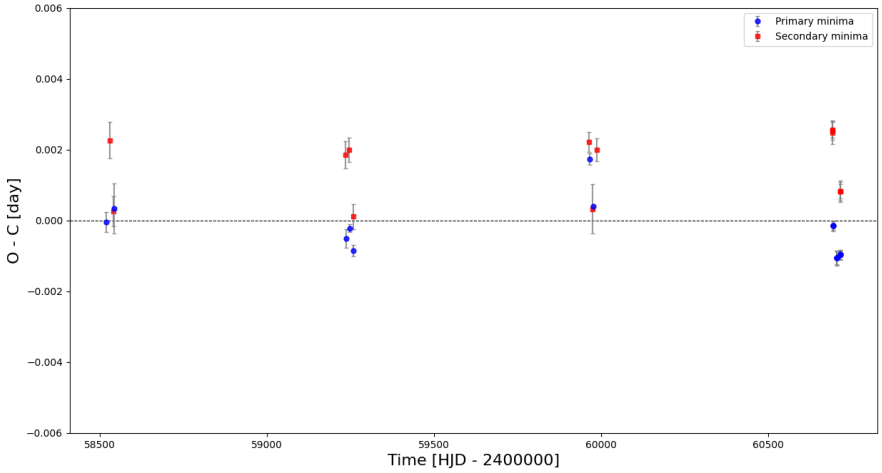

Figure 4.9: 2MASS J08453462-2158013 $O-C$ diagram.

Parameter	Old value	New value
P	11.0420	11.0418(8)
M_0	54402.438	58519.079(1)

Table 4.8: Adjusted ephemerides for 2MASS J08453462-2158013. M_0 is in HJD-2400000.

4.2.3 V919 Cep

Even at first glance on the Figure 4.10, the binary system V919 Cep is undergoing evolution and changes. It was possible to identify and model the apsidal motion, that is typical of eccentric binaries. The apsidal motion can be seen in the diagram as two sine waves in antiphase. The entire plane of the orbit is rotating, so from our perspective, the positions of the primary and secondary eclipses change.

For the construction of the diagram, the data were supplemented with observations from MMT9 (Biryukov et al., 2015) and VarAstro (Sekce proměnných hvězd a exoplanet ČAS, 2023), which extend further back in time and thus helped to better determine the apsidal motion.

For this system, adjusting the ephemerides is more complicated because they are constantly changing due to the apsidal motion. The adjusted values differ insignificantly and are valid only for a limited time.

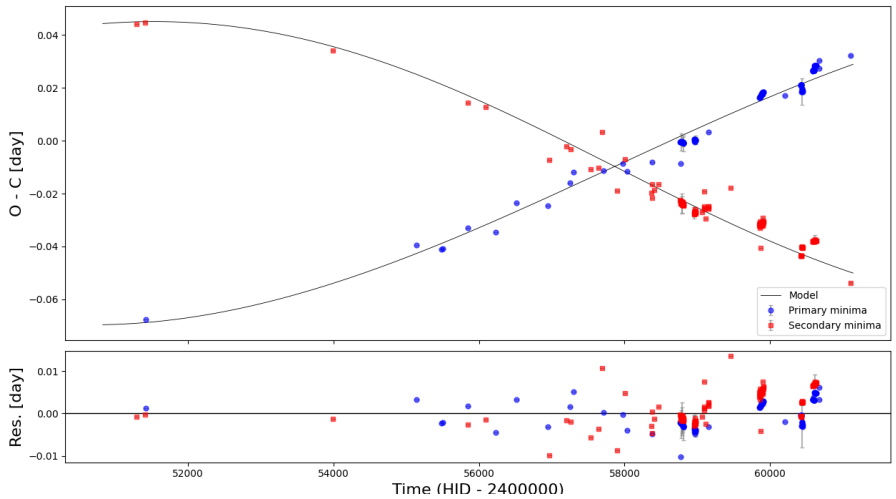

Figure 4.10: V919 Cep $O-C$ diagram with apsidal motion model.

Parameter	Old value	New value
P	1.851982	1.851983(1)
M_0	58765.761	58765.752(1)

Table 4.9: Adjusted ephemerides for V919 Cep. M_0 is in HJD-2400000.

Apsidal motion is directly linked to the internal structure constant (ISC) k_2, a value that determines the distribution of mass within stars. Mean value of ISC can be calculated from classical component of rate of apsidal motion $\dot{\omega}_{\rm cl}$ and geometric coefficient $c_{\rm cl}$ as (Claret and Gimenez, 1993):

$$\bar{k}_{2,\rm obs} = \frac{\dot{\omega}_{\rm cl}}{c_{\rm cl}}. \tag{4.2}$$

Parameter	Value
P	1.85189(4) d
e	0.088(1)
r_1	0.22(1)
r_2	0.18(1)
$q = M_2/M_1$	0.73(1)
U	74.1(5) yr
$\dot{\omega}_{\rm obs}$	$4.30(2) \times 10^{-4}$ rad/cycle
$\log(k_{2,\rm obs})$	−2.18(3)

Table 4.10: Parameters used in calculations and results.

Table 4.10 includes the system parameters required for the calculation as well as the resulting ISC value. The r_i is R_i/a, U is the period of apsidal motion, and the rate of apsidal rotation is given by the equation:

$$\dot{\omega}_{\rm obs} = \frac{360}{U} = 4.86 \text{ deg/yr} = 4.30 \times 10^{-4} \text{ rad/cycle}. \tag{4.3}$$

Because of the elliptical orbits, the eccentricity must also be included in the calculation using Sterne's factor $f(e)$ (Sterne, 1939). However, in our case of low eccentricity, the correction using this function will be minimal:

$$f(e) = \frac{1 + \frac{3}{2}e^2 + \frac{1}{8}e^4}{(1-e^2)^5} = 1.0518, \tag{4.4}$$

$$c_{21} = 15\frac{M_2}{M_1}r_1^5 f(e) = 0.00538, \tag{4.5}$$

$$c_{22} = 15\frac{M_1}{M_2}r_2^5 f(e) = 0.00341, \tag{4.6}$$

where c_{2i} are geometric coefficients representing the deformation of stars due to tidal forces for each component separately. Therefore, for the system as a whole, this gives:

$$c_{\text{tide}} = c_{21} + c_{22} = 0.00879. \tag{4.7}$$

Synchronized rotation was also assumed in the physical modelling, so we can assume it now as well, and therefore we can write:

$$c_{\text{rot},i} = \frac{1}{(1-e^2)^2}r_i^5\left(1 + \frac{M_{3-i}}{M_i}\right), \tag{4.8}$$

where $(1-e^2)^{-2} = g(e)$ is Sterne's factor for rotation.

$$c_{\text{rot},1} = 0.00082 \tag{4.9}$$

$$c_{\text{rot},2} = 0.00038 \tag{4.10}$$

$$c_{\text{rot}} = c_{\text{rot},1} + c_{\text{rot},2} = 0.00120 \tag{4.11}$$

Total contribution of a classical member:

$$c_{\text{cl}} = c_{\text{tide}} + c_{\text{rot}.} = 0.00999. \tag{4.12}$$

Relativistic contribution:

$$\dot{\omega}_{\text{GR}} = 5.45 \times 10^{-4}\frac{1}{(1-e^2)}\left(\frac{M_1 + M_2}{P}\right)^{2/3}, \tag{4.13}$$

$$\dot{\omega}_{\text{GR}} \approx 5.3 \times 10^{-6}\ \text{rad/cycle}. \tag{4.14}$$

Only the classical contribution affects the mass inside stars and thus k_2 itself. Therefore, we must subtract the contribution of the apsidal motion caused by the curvature of spacetime:

$$\dot{\omega}_{\text{cl}} = \dot{\omega}_{\text{obs}} - \dot{\omega}_{\text{GR}}, \tag{4.15}$$

$$\dot{\omega}_{\rm cl} = 3.92 \times 10^{-4}\ \mathrm{rad/cycle}. \tag{4.16}$$

Based on the previous results, the ISC can be quantified as:

$$\bar{k}_{2,\rm obs} = \frac{\dot{\omega}_{\rm cl}}{c_{\rm cl}} = 0.0066 \pm 0.0001 \tag{4.17}$$

$$\log(\bar{k}_{2,\rm obs}) = -2.18 \pm 0.03 \tag{4.18}$$

The calculated value is consistent with the assumption that these are main-sequence stars with an uneven distribution of mass. The stars have a very dense core, and the density decreases toward the surface, ending in a very thin atmosphere.

According to Claret (2004), the theoretical ISC values for systems similar to these $M = 2.5\,M_{\odot}$ are $\log(k_{2,\rm theo}) \approx -2.10$, so the values differ slightly. A significant percentage of the uncertainty stems from the determination of relative radii (r^5) as well as the determination of masses. A lower calculated value could also mean that the stars have already undergone some evolution, and the distribution of mass has changed slightly.

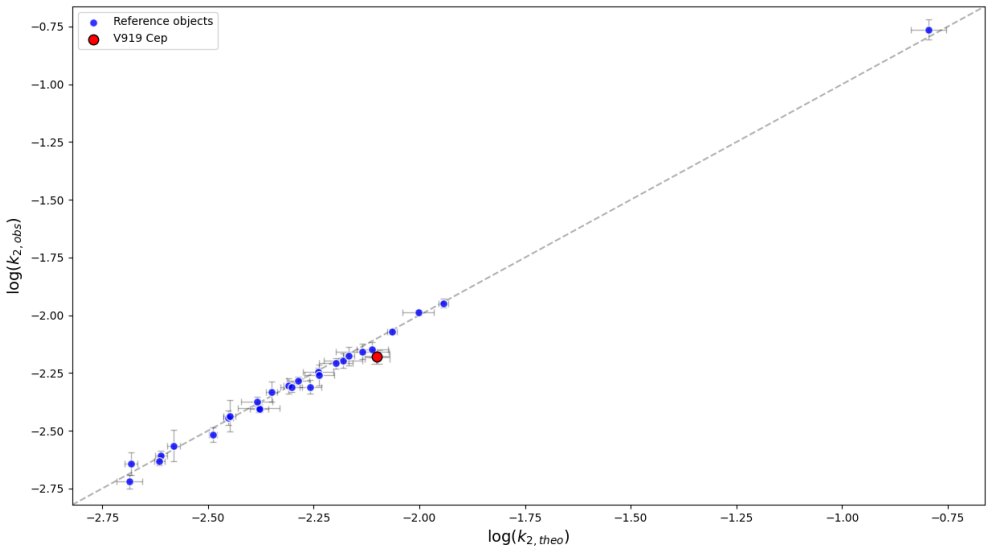

Figure 4.11: Comparison of the ISC calculated for V919 Cep and reference objects from the study Claret et al. (2021).

Figure 4.11 shows V919 Cep in comparison with other objects exhibiting apsidal motion for which the ISC has been calculated. The graph plots the relationship between the observed $k_{2,\rm obs}$ and the theoretical $k_{2,\rm theo}$. Since the values should be identical, a linear relationship is expected. It can be seen that all points, including V919 Cep, satisfy this assumption. The slight deviation of the object under study may be due to a lack of information about the system, as it may be in a different evolutionary stage, and also because the $k_{2,\rm theo}$ was estimated from tables that include masses and metallicity. These values could not be derived and are therefore estimated based on the assumed stage of evolution.

4.2.4 AT Lep

In addition to the two data sources used for all objects, another source, SuperWASP (Thiemann et al., 2022) was added here, providing older observations than those previously available from TESS and ASAS-SN.

It was not possible to extract the times of the secondary minima from the SuperWASP data. This was due to the absence of complete secondary minima. Furthermore, the results obtained from the model were highly inaccurate. Nevertheless, these measurements provided new insights into the system by revealing a possible period change that was previously unidentifiable.

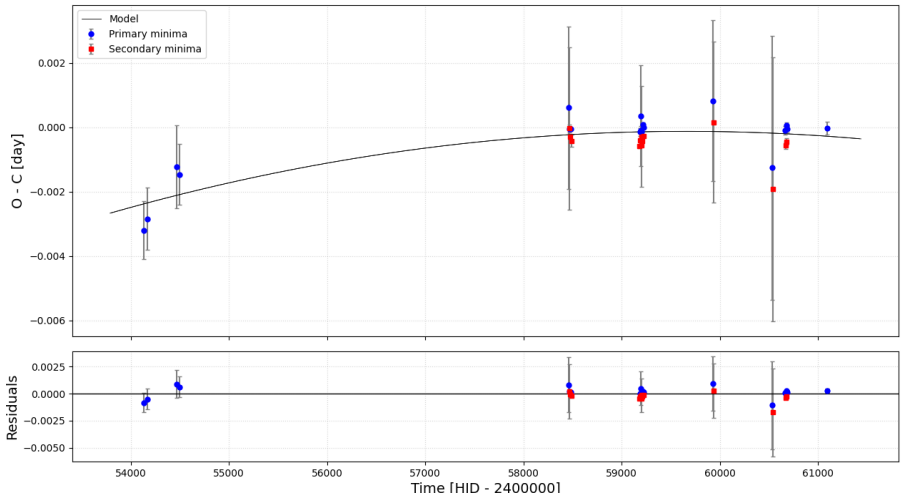

Figure 4.12: AT Lep $O-C$ diagram with a sign of a period change.

The $O-C$ diagram revealed a concave parabolic shape, indicating a shortening of the period. The results are presented in Table 4.11. The period gets shorter by about 0.05 seconds per year. Further observations would be useful to confirm whether the changes in the system are real, but such observations were not available.

Parameter	Old value	New value
P	10.6495	10.6494(1)
M_0	52634.523	52506.995(2)
	Value	Error
dP [day/yr]	$5.75 \cdot 10^{-7}$	$3.51 \cdot 10^{-7}$
dP [s/yr]	0.05	0.03

Table 4.11: Adjusted ephemerides for AT Lep with results of the fit for period change in the system.

4.2.5 CF Mon

Based on available observations, the CF Mon system shows no evolution or change. Although some points lie outside the zero line, they are still within the margin of deviation.

If we were to consider only the data from TESS, for which three sectors are available, the system would undergo a very rapid change in period. However, after including observations from ASAS-SN, the picture changes because the only inconsistency is a group of points belonging to a single sector from TESS. These points deviate from the others even though the error bars indicate that they were determined accurately. A likely explanation is a systematic measurement error, which cannot be confirmed from the available information. Further observations would be needed to confirm these assumptions.

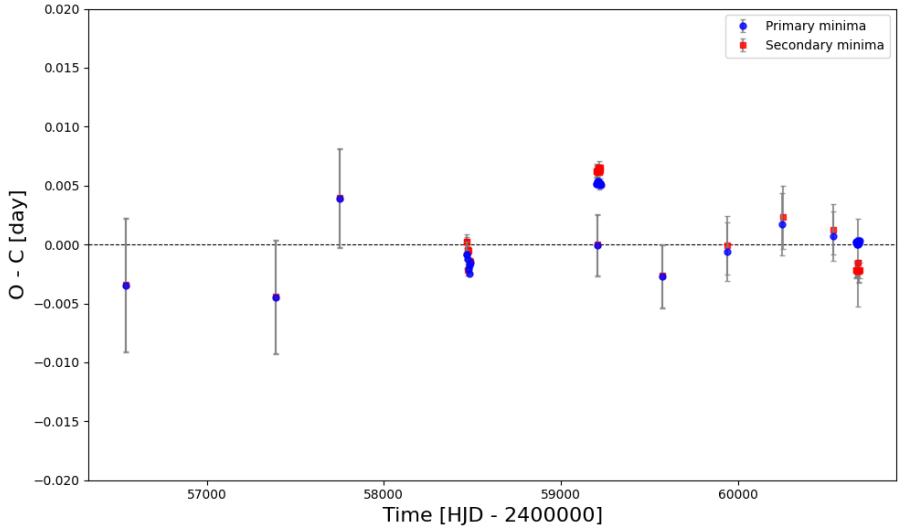

Figure 4.13: CF Mon $O-C$ diagram.

Parameter	Old value	New value
P	2.6105	2.6104(1)
M_0	30049.203	30047.466(5)

Table 4.12: Adjusted ephemerides for CF Mon. M_0 is in HJD-2400000.

4.3 Period - eccentricity diagram

Based on current knowledge, it is highly likely that all binary star systems will eventually reach circular orbits. Tidal forces change due to eccentricity, and as a result, the mechanical energy of the stars' rotation is dissipated and converted into heat. This leads to the gradual circularization of the orbits. The relationship between eccentricity and orbital period is used to study the effect of circularization. A statistical representation of this dependence is called a *P-e* diagram. Systems in which components are close together are much more susceptible to the circularization process than detached systems with large distances between stars and long periods. It follows that the relative size of the stars (R/a) is a very important parameter (Zahn and Bouchet, 1989). The $P-e$ diagram can also be used to estimate the ages of stellar systems and clusters. If a system with a short period continues to orbit with a non-zero eccentricity, it means that circularization has not yet occurred and,

therefore, that the system is likely still quite young. This method is particularly useful for star clusters. Young globular clusters exhibit a significantly lower P_{circ} value (1–2 days) than older open clusters, where P_{circ} can reach tens of days. P_{circ} is the critical orbital period below which a system is always circular (Meibom and Mathieu, 2005).

Figure 4.14 shows the binary stars studied in this thesis. Additional objects have been included for comparison and to provide a more representative sample. Comparison objects were taken from Kim et al. (2018) and Zasche et al. (2021).

A trend is evident across the entire sample: objects with longer periods typically have greater eccentricity, as they are less susceptible to tidal forces. The objects under study fit within the comparison distribution, and there are no outliers. The three red objects lie almost in a straight line with a period of $\log P \approx 1$ d, but with completely different eccentricities. This could mean that they are at different stages of circularization. Object (4) has a long period and low eccentricity, so it is likely older than object (2), which, according to the comparison sample, is probably approaching the upper limit of eccentricity for this period.

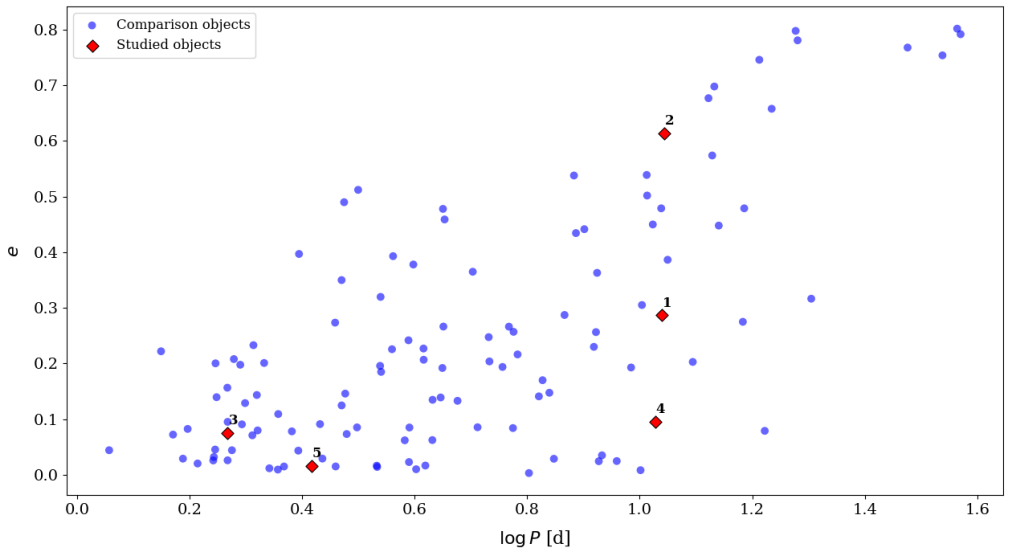

Figure 4.14: *P-e* diagram. Marked objects: (1) 2MASS J10024347-5643283, (2) 2MASS J08453462-2158013, (3) V919 Cep, (4) AT Lep, (5) CF Mon.

Conclusion

This thesis focused on the study of five eclipsing binary stars with non-zero eccentricity orbits. Available photometric data were analyzed. The main source was the TESS satellite, supplemented by the ASAS-SN survey and others. Own observations were also made, resulting in a few minima timings for: CF Mon, AT Lep, and V919 Cep. However, mainly due to the period length and position of some objects, it was not possible to obtain complete light curves. Some of the available data were not used because they were inaccurate and clearly influenced the results, or because it was not possible to construct light curves at all.

The minima times were determined from the photometric data, and $O-C$ diagrams were constructed. All the minima timings used in the research will be attached to the thesis in electronic form (or on: github.com/SamuelFabo/Diploma-thesis-data.git). The $O-C$ diagrams were analyzed for all objects, and where possible, the ephemerides were fitted and corrected. AT Lep exhibits a slow period change d$P = 0.05$ s/yr, but additional data would be needed for full confirmation. Apsidal motion with period of 74.1 yr was identified in the V919 Cep system. Sufficient data allowed for the fitting of this phenomenon and the determination of the parameters needed to calculate the internal structure constants ($\log(k_{2,\mathrm{obs}}) = -2.18$). The calculated value was compared with the theoretical value. It is in good agreement with the other objects as displayed in Figure 4.11. In other systems, the period appears to be constant so far. However, the short duration of high-quality observations was an issue, which prevented a more detailed analysis of the period's evolution.

Physical models were calculated for the systems under study. Since only photometric data were available, only some parameters could be determined. The eccentricity was confirmed and calculated for all systems. The values extend from nearly circular orbits ($e = 0.016$) to highly eccentric orbits ($e = 0.613$). Initially, a sign of pulsation was detected in the 2MASS J08453462-2158013 system. Detailed analysis revealed the source of the pulsations to be a neighboring star in the field, which contaminated the photometry of 2MASS J08453462-2158013. The CF Mon model was complicated by the asymmetry of the eclipses and the presence of a third light. The q value is also questionable, as it suggests that the secondary component should be more massive, yet the model predicts a much lower temperature for it. Except for CF Mon, the components of the binaries appear to be on the main sequence. All phase curves are of the Algol-type, and according to the models, these are likely separate systems. A *P-e* diagram was constructed. The objects cover a relatively wide range of periods and eccentricities, and each appears to be at a different stage of evolution. In the diagram (Fig. 4.14), they were compared with other eccentric binary stars.

Eccentric binary stars generally require long-term photometric observations to confirm period changes or unveil a new one. Spectroscopic observations would also be necessary to calculate radial velocities and absolute parameters of the binary components.

Appendix

An electronic appendix, uploaded to the IS MU system, containing the minima timings used, will be attached to this thesis. Also available on: github.com/SamuelFabo/Diploma-thesis-data.git.

q-search

This method was used to find the most likely values of the q-parameter. In the PHOEBE program, the value of q was repeatedly changed, and the other parameters were fitted so that the resulting χ^2 value was as small as possible.

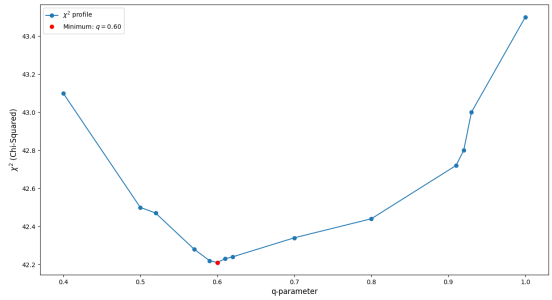

Figure 4.15: 2MASS J10024347-5643283

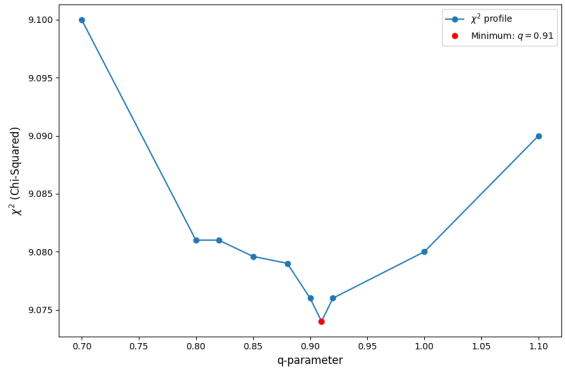

Figure 4.16: 2MASS J08453462-2158013

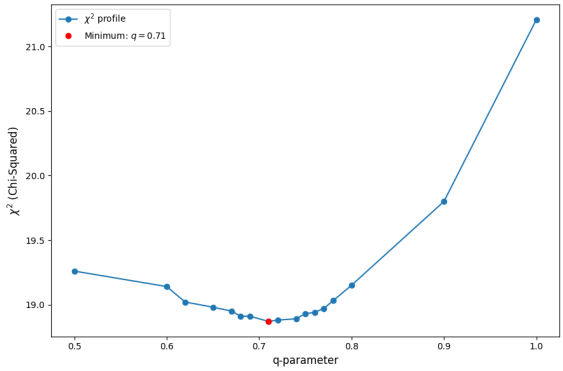

Figure 4.17: V919 Cep

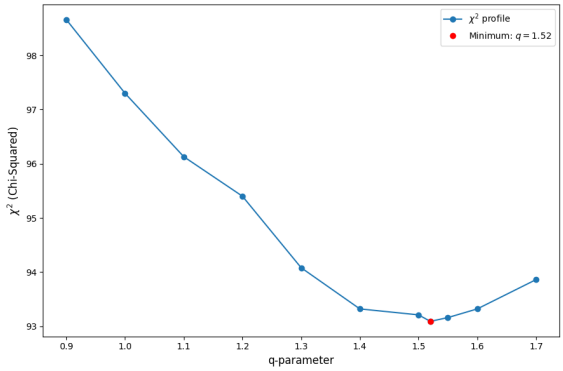

Figure 4.18: CF Mon

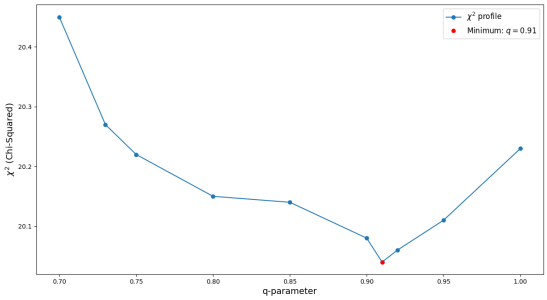

Figure 4.19: AT Lep.

Bibliography

AAVSO. The aavso international database. American Association of Variable Star Observers, https://www.aavso.org, 2024.

Australian Telescope National Facility. Introduction to Binary Stars. URL https://www.atnf.csiro.au/outreach/education/senior/astrophysics/binary_intro.html. Accessed: 2026-03-26.

A. Bayo, C. Rodrigo, D. Barrado y Navascués, E. Solano, R. Gutiérrez, M. Morales-Calderón, and F. Allard. Vosa: Virtual observatory sed analyzer. *Astronomy & Astrophysics*, 492:277–287, 2008. doi: 10.1051/0004-6361:200810395.

E. C. Bellm, S. R. Kulkarni, M. J. Graham, et al. The zwicky transient facility: System overview, performance, and first results. *Publications of the Astronomical Society of the Pacific*, 131(995):018002, 2019. doi: 10.1088/1538-3873/aaecbe.

A. Biryukov, G. Beskin, S. Karpov, S. Bondar, E. Ivanov, E. Katkova, A. Perkov, and V. Sasyuk. The first light of Mini-MegaTORTORA wide-field monitoring system. *Baltic Astronomy*, 24:100–108, Jan. 2015. doi: 10.1515/astro-2017-0208.

E. Budding and O. Demircan. *Introduction to Astronomical Photometry*, volume 6. 2007.

K. C. Chambers, E. A. Magnier, N. Metcalfe, et al. The pan-starrs1 surveys. *arXiv e-prints*, page arXiv:1612.05560, 2016.

F. Chromey. *To Measure the Sky: An Introduction to Observational Astronomy*. Cambridge University Press, 2010. ISBN 9780521763868. URL https://books.google.sk/books?id=OB29T2BWLD4C.

A. Claret. The dependence of the apsidal-motion constants on stellar evolution. *Astronomy & Astrophysics*, 424:919–925, 2004. doi: 10.1051/0004-6361:20041141.

A. Claret. New grids of stellar models including tidal-evolution constants up to carbon burning. I. From 0.8 to 125 M at Z=0.02. , 424:919–925, Sept. 2004. doi: 10.1051/0004-6361:20040470.

A. Claret and A. Gimenez. The apsidal motion test of the internal stellar structure : comparison between theory and observations. , 277:487–502, Oct. 1993.

A. Claret and A. Gimenez. The apsidal-motion test of stellar structure and evolution: an update. *Astronomy and Astrophysics*, Sept. 2010. doi: 10.1051/0004-6361/201014008.

A. Claret, A. Giménez, D. Baroch, I. Ribas, J. C. Morales, and G. Anglada-Escudé. Analysis of apsidal motion in eclipsing binaries using TESS data. II. A test of internal stellar structure. , 654:A17, Oct. 2021. doi: 10.1051/0004-6361/202141484.

P. P. Eggleton. Aproximations to the radii of Roche lobes. , 268:368–369, May 1983. doi: 10.1086/160960.

M. Fiorucci and U. Munari. The Asiago Database on Photometric Systems (ADPS). II. Band and reddening parameters. , 401:781–796, Apr. 2003. doi: 10.1051/0004-6361:20030075.

A. Frigo and F. Giordani. Studio fotometrico della binaria. *Ann. Mus, Civ. Rovereto*, 18: 213–233, 2003.

M. Fukugita, T. Ichikawa, J. E. Gunn, M. Doi, K. Shimasaku, and D. P. Schneider. The Sloan Digital Sky Survey Photometric System. , 111:1748, Apr. 1996. doi: 10.1086/117915.

Gaia Collaboration, A. Vallenari, A. G. A. Brown, T. Prusti, and J. H. J. de Bruijne. Gaia Data Release 3. Summary of the content and survey properties. , 674:A1, June 2023. doi: 10.1051/0004-6361/202243940.

P. Gajdoš and Š. Parimucha. New tool with GUI for fitting O-C diagrams. *Open European Journal on Variable Stars*, 197:71, Apr. 2019.

H. Goldstein, C. Poole, and J. Safko. *Classical Mechanics (3rd Edition)*. 06 2001. ISBN 0201657023.

A. A. Henden, S. Levine, D. Terrell, and D. L. Welch. Apass - the latest data release. In *American Astronomical Society Meeting Abstracts #225*, volume 225 of *American Astronomical Society Meeting Abstracts*, page 336.16, 2015.

R. W. Hilditch. *An Introduction to Close Binary Stars*. 2001.

S. B. Howell. *Handbook of CCD Astronomy*, volume 5. 2006.

H. Johnson and W. Morgan. Fundamental stellar photometry for standards of spectral type. *Astrophysical journal*, 1953.

C. H. Kim, J. M. Kreiner, and B. Zakrzewski. A Comprehensive Catalog of Galactic Eclipsing Binary Stars with Eccentric Orbits Based on Eclipse Timing Diagrams. , 235 (2):41, Apr. 2018. doi: 10.3847/1538-4365/aab7ef.

C. S. Kochanek, B. J. Shappee, K. Z. Stanek, T. W.-S. Holoien, T. A. Thompson, J. L. Prieto, S. Dong, J. V. Shields, D. Will, C. Britt, D. Perzanowski, and G. Pojmański. The All-Sky Automated Survey for Supernovae (ASAS-SN) Light Curve Server v1.0. , Oct. 2017. doi: 10.1088/1538-3873/aa80d9.

Z. Kopal. *Close binary systems*. 1959.

Lightkurve Collaboration, J. V. d. M. Cardoso, C. Hedges, M. Gully-Santiago, and et al. Lightkurve: Kepler and TESS time series analysis in Python. Astrophysics Source Code Library, record ascl:1812.013, Dec. 2018.

H. Maehara. Kamogata/kiso/kyoto wide-field survey (kws). *Journal of Space Science Informatics Japan*, 3:119–127, 2014.

J. M. Mas-Hesse, A. Giménez, J. L. Culhane, et al. The optical monitoring camera on integral. standard and fast photometry. *Astronomy & Astrophysics*, 411:L261–L267, 2003. doi: 10.1051/0004-6361:20031314.

T. Mazeh. Observational evidence for tidal interaction in close binary systems. *EAS Publications Series*, 29:1–65, 2008. ISSN 1638-1963. doi: 10.1051/eas:0829001. URL `http://dx.doi.org/10.1051/eas:0829001`.

S. Meibom and R. D. Mathieu. A robust measure of tidal circularization in coeval binary populations: The solar-type spectroscopic binary population in the open cluster m35*. *The Astrophysical Journal*, 620(2):970, feb 2005. doi: 10.1086/427082. URL `https://doi.org/10.1086/427082`.

Z. Mikulášek. Phenomenological modelling of eclipsing system light curves. , 584:A8, Dec. 2015. doi: 10.1051/0004-6361/201425244.

MUST. Mikulski archive for space telescopes. https://archive.stsci.edu/; (Accessed: 2026-04-24).

NASA. Nasa exoplanet archive. https://exoplanetarchive.ipac.caltech.edu/; (Accessed: 2026-04-24).

NASA HEASARC. Nasa tess science support center. /heasarc.gsfc.nasa.gov/ (Accessed: 14-2-2025).

NASA/IPAC Infrared Science Archive. Infrared science archive (irsa). California Institute of Technology, 2024. URL `https://irsa.ipac.caltech.edu/`.

M. J. Pecaut and E. E. Mamajek. Intrinsic Colors, Temperatures, and Bolometric Corrections of Pre-main-sequence Stars. , 208(1):9, Sept. 2013. doi: 10.1088/0067-0049/208/1/9.

O. Pejcha. Světelné křivky z TESS. *Sekce proměnných hvězd a exoplanet ČAS*, Nov. 2020. URL `https://www.youtube.com/watch?v=47g7ypzHTRI`. Provided by the SAO/NASA Astrophysics Data System.

O. Pejcha, P. Cagas, C. Landri, M. Fausnaugh, and Z. Henzl. The complex dynamical past and future of double eclipsing binary czev343: Misaligned orbits and period resonance. *A&A*, 667:A53, 2022. doi: 10.1051/0004-6361/202244335. URL `https://doi.org/10.1051/0004-6361/202244335`.

J. R. Percy. Understanding Variable Stars. *Cambridge University Press*, 2007.

A. Prša and T. Zwitter. A Computational Guide to Physics of Eclipsing Binaries. I. Demonstrations and Perspectives. , 628(1):426–438, July 2005. doi: 10.1086/430591.

G. R. Ricker, J. N. Winn, and R. Vanderspek. Transiting Exoplanet Survey Satellite (TESS). *Journal of Astronomical Telescopes, Instruments, and Systems*, 1:014003, Jan. 2015. doi: 10.1117/1.JATIS.1.1.014003.

H. Sana and J. Vrancken. Observing Binaries. *arXiv e-prints*, Apr. 2025. doi: 10.48550/arXiv.2504.00548.

Sekce proměnných hvězd a exoplanet ČAS. Varastro. `http://var.astro.cz/`, 2023.

C. Sterken. The o-c diagram: Basic procedures. *The Light-Time Effect in Astrophysics, Proceedings of ASP Conference Series*, 335:3–11, 2005. doi: 2005ASPC..335....3S.

T. E. Sterne. Apsidal motion in binary stars. , 99:451–462, Mar. 1939. doi: 10.1093/mnras/99.5.451.

T. M. Tauris and E. P. J. van den Heuvel. *Physics of Binary Star Evolution. From Stars to X-ray Binaries and Gravitational Wave Sources*. 2023. doi: 10.48550/arXiv.2305.09388.

H. Thiemann, A. J. Norton, U. C. Kolb, H. J. Dickinson, and A. McMaster. SuperWASP Variable Stars: Classifying Light Curves Using Citizen Science. In J. E. Ruiz, F. Pierfedereci, and P. Teuben, editors, *Astronomical Data Analysis Software and Systems XXX*, volume 532 of *Astronomical Society of the Pacific Conference Series*, page 303, July 2022.

J. L. Tonry, L. Denneau, A. N. Heinze, B. Stalder, K. W. Smith, S. J. Smartt, C. W. Stubbs, H. J. Weiland, and A. Rest. ATLAS: A High-cadence All-sky Survey System. , 130 (988):064505, June 2018. doi: 10.1088/1538-3873/aabadf.

G. Torres, J. Andersen, and A. Giménez. Accurate masses and radii of normal stars: modern results and applications. , 18(1-2):67–126, Feb. 2010. doi: 10.1007/s00159-009-0025-1.

C. Watson and AAVSO. The international variable star index (vsx). url: vsx.aavso.org (Accessed: 2026-05-03).

R. E. Wilson and E. J. Devinney. Realization of Accurate Close-Binary Light Curves: Application to MR Cygni. , 166:605, June 1971. doi: 10.1086/150986.

J. Wright and B. Gaudi. Exoplanet detection methods. *Planets, Stars and Stellar Systems. Volume 3: Solar and Stellar Planetary Systems*, 10 2012. doi: 10.1007/978-90-481-8818-5˙59.

J.-P. Zahn and L. Bouchet. Tidal evolution of close binary stars. II. Orbital circularization oflate-type binaries. , 223:112–118, Oct. 1989.

P. Zasche, Z. Henzl, and M. Mašek. Hunt for extremely eccentric eclipsing binaries. , 652: A81, Aug. 2021. doi: 10.1051/0004-6361/202141052.